August 2014

Zebrafish as a Model for Determining the Mechanisms Causing Deafness in MYH9-Related Disease

Luke David Spychalla
University of Wisconsin-Milwaukee

ZEBRAFISH AS A MODEL FOR DETERMINING THE MECHANISMS CAUSING DEAFNESS IN *MYH9*-RELATED DISEASE

by

Luke Spychalla

A Thesis Submitted in

Partial Fulfillment of the

Requirements for the Degree of

Master of Science

in Biological Sciences

at

The University of Wisconsin-Milwaukee

August 2014

ABSTRACT

ZEBRAFISH AS A MODEL FOR DETERMINING THE MECHANISMS CAUSING DEAFNESS IN *MYH9*-RELATED DISEASE

by

Luke Spychalla

The University of Wisconsin-Milwaukee, 2014
Under the Supervision of Dr. Jennifer Gutzman, Ph.D.

Approximately 1 in 500 infants are diagnosed with hearing loss, and about half of these cases can be traced to genetic defects. Several hundred genes have been implicated in deafness, including *MYH9*, which codes for the conventional motor protein non-muscle myosin IIA (NMIIA). Mutations in *MYH9* lead to syndromic *MYH9*-related diseases, which include deafness as a variable symptom, as well as non-syndromic autosomal deafness DFNA17. Despite its identification as a deafness gene, the functions of *MYH9* in ear development and hearing remain unknown. To study this role, we will use zebrafish as a model. Zebrafish offer significant advantages including established genetic tools, large clutch sizes, and transparent embryos that develop externally. In addition, non-muscle myosin genes, including *MYH9*, are highly conserved from zebrafish to human, and the development and function of the vertebrate ear is also highly conserved. Zebrafish share many inner ear structures with humans including the sensory hair cells and cilia that make vestibular and auditory function possible. We hypothesize that *myh9* plays a significant role in the developing zebrafish ear as suggested by *myh9* knockdown experiments, which resulted in the phenotype

of an abnormal number of otoliths. Because otoliths nucleate from precursor particles distributed in the fluid of the otic vesicle by motile cilia, we further hypothesize that the otolith phenotype is caused by a cilia defect. Our work has demonstrated that NMIIA colocalizes with ciliary basal bodies in the otic vesicle, suggesting a possible role in establishing basal body orientation.

To Mary K. Selig, whose unfaltering care and support helped make this thesis possible

TABLE OF CONTENTS

LIST OF FIGURES

LIST OF TABLES

Chapter 1: Introduction

A. General Introduction

In humans, mutations in the *MYH9* gene encoding the well-conserved actin motor protein non-muscle myosin IIA (NMIIA) result in a host of disorders, collectively known as *MYH9*-related diseases. These consist of May-Hegglin anomaly, Fechtner Syndrome, Sebastian Syndrome, and Epstein Syndrome, with symptoms including platelet abnormalities, nephritis, visual defects, and sensorineural deafness (Heath et al., 2001). There are five known mutations in *MYH9* that are associated with syndromic deafness, and there is a single point mutation in *MYH9* which causes nonsyndromic deafness DFNA17 (Lalwani et al., 2000; Seri et al., 2000).

We are using the zebrafish as a model system to determine the role of *MYH9* in the formation and function of the ear as an initial step to determine the mechanisms leading to deafness in human *MYH9*-related diseases. One specific advantage of using zebrafish is the conservation of anatomy and physiology of the vertebrate inner ear structures (Thomas et al., 2013). In addition, zebrafish have easily-accessible hair cells in their ear during development as well as in the lateral line, a sensory system consisting of clusters of hair cells called neuromasts used to sense displacement of water outside the body (Ghysen & Dambly-Chaudiere, 2007). There is high sequence identity between human and zebrafish *MYH9* genes (table 1), and there are ample tools available to manipulate *myh9* genetically in zebrafish, such as short antisense oligonucleotides for gene knockdown (Schartl, 2014). Zebrafish embryos are

transparent in early development, mature externally, and are born in large clutches, making them ideal for studying the development and function of the ear and potentially useful as a drug screening tool in the future.

B. Myosin II Structure and Function.

The *MYH9* gene mutated in *MYH9*-related diseases encodes for non-muscle myosin IIA. Non-muscle myosins make up just one portion of the class II myosins. The myosin proteins in general are a superfamily of 35 classes of motor proteins that share the property of force transduction through ATP hydrolysis in order to move along actin filaments (Odronitz & Kollmar, 2007). Myosins are classified into two categories. The first is conventional class II myosins and the second is unconventional myosins, which includes all other myosin classes. These large families of proteins have diverse and highly conserved roles across the kingdoms, ranging from trafficking of cargo (Odronitz & Kollmar, 2007), to cytokinesis (Scholey, Brust-Mascher, & Mogilner, 2003), to maintenance of cell shape (Yumura & Uyeda, 2003). Conventional myosin II is divided into two groups of proteins based on function. The first is muscle myosin II proteins which serve as contractile elements of the sarcomere in fibers of cardiac, smooth and skeletal muscle and the second is non-muscle myosin II (NMII) proteins which carry out a variety of intracellular functions including cell migration, cell division, and cell shape changes through interaction with the actin cytoskeleton (Lo et al., 2004; Saitoh et al., 2001; Svitkina et al., 1997). NMII exists in three isoforms: non-muscle myosin II A, B, and C, encoded by the genes *MYH9*, *MYH10* and

MYH14, respectively; however, only mutations in *MYH9* lead to *MYH9*-related diseases.

Several specific functions for NMIIA have been characterized. Related to its ability to bind actin are several roles pertaining to cytoskeleton binding, including maintenance of cellular shape and organization, cell migration, and cytokinesis (Heath et al., 2001). Combining this cytoskeletal binding function of NMIIA with the ability to interact with cargo at its tailpiece also allows it to move organelles and vesicles within the cytosol and for endo- and exocytosis (Ricketson, Johnston, & Prehoda, 2010).

The NMII isoforms share the structural configuration of being hexameric two-headed proteins composed of a heavy chain dimer and two pairs of light chains to yield a bipolar structure (Fig. 1) (reviewed by Eddinger & Meer, 2007). The N-terminus contains two globular heads that serve as the domains responsible for actin binding and ATP hydrolysis to generate motion. Adjacent to the head domain is the neck domain, a linking region of the protein that acts as a lever arm to transduce the force generated at the motor heads to the power stroke that moves the entire protein along actin. The neck domain is also the site of association for a pair of regulatory light chains, which regulate NMII activity, and a pair of essential light chains, which stabilize the heavy chain structure (Conti & Adelstein, 2008; Vicente-Manzanares et al., 2009). At the C-terminal end of the dimer is a single rod domain composed of alpha helices. These are arranged in a coiled-coil motif which allows for the myosin monomers to polymerize into bipolar filaments. At the end of the rod domain is a short non-

helical tailpiece that is able to bind cargo molecules and potentially interact with other myosin molecules (Sanborn et al., 2011). Of these regions, mutations in the head domain result in the most deleterious deafness phenotypes, specifically in a subdomain called the SH1 helix which composes a joint connecting other head subdomains (Iwai, Hanamoto, & Chaen, 2006; Murayama et al., 2013).

Studies in mouse have found *myh9* expression throughout auditory hair cells, including the apical membrane, cytosol, stereocilia and mitochondria (Mhatre et al., 2006). In zebrafish we have demonstrated that NMIIA is expressed throughout the embryo from the onset of ear development (Gutzman et al., in review). Although *myh9* expression has been found in the ear in multiple model systems, the role for *myh9* in development and function of the ear is unknown.

C. *MYH9*-Related Disease and the Mutations that Cause Deafness

Disease associated with mutations in *MYH9* can be categorized as syndromic or nonsyndromic. Currently, there is only one disorder associated with *MYH9* that is nonsyndromic: autosomal dominant nonsyndromic deafness 17 (DFNA17). DFNA17 is known to result in sensorineural hearing loss with an onset of high frequency hearing loss at ten years of age that degenerates to severe deafness at all frequencies near age thirty (Lalwani et al., 1999), and does not have the hematological symptoms common in *MYH9* syndromic diseases (Lalwani et al., 2000). *MYH9* syndromic disease includes four similar disorders that are collectively called *MYH9*-related disease, and which share the properties of being rare and heritable in an autosomal dominant fashion (Heath

et al., 2001). The names of these diseases are May-Hegglin anomaly, Fechtner Syndrome, Sebastian Syndrome, and Epstein Syndrome.

Symptoms of *MYH9*-related diseases typically include the hematological conditions of macrothrombocytopenia and leukocyte inclusion bodies (Mhatre et al., 2007). There are also a set of variable symptoms associated with *MYH9*-related disease which include glomerulonephritis, sensorineural deafness, and presenile cataracts (Heath et al., 2001). The reason for the relative invariability of hematological symptoms over these variable ones is that hematopoietic cells express *MYH9* only, and not the isoforms of *MYH10* or *MYH14*. NMIIB and NMIIC may compensate for reduced or ineffective NMIIA in tissues susceptible to variable symptoms such as the kidney, inner ear, and eye (Heath et al., 2001). Additionally, it is believed that unknown genetic, epigenetic and environmental factors may play a role in *MYH9*-related disease phenotypes (Heath et al., 2001).

To date, 45 mutations in *MYH9* have been identified in the human population, 80% of which are clustered in 6 of the 40 *MYH9* exons (Iwai et al., 2006). The most frequent specific mutations are R702C, D1424N, E1841K, and R1933X (Fig. 1) (Heath et al., 2001). Of these known mutations, several have been associated with definite or variable risk of syndromic or non-syndromic hearing loss (Heath et al., 2001). Generally, mutations in the NMIIA head domains result in the most severe hearing phenotypes. It is hypothesized that these mutations are more severe because they destabilize the SH1 helix that acts as a joint between other head domains (Iwai et al., 2006). These include the mutations Arg702 (R702C and R702H) which results in hearing impairment in

early infancy that degenerates to full deafness in adolescence (Kunishima & Saito, 2010), and R705H, which causes autosomal dominant nonsyndromic deafness DFNA17 (Fig. 1) (Kunishima & Saito, 2010). While these *MYH9* mutations are known to be associated with deafness, the role for *MYH9* in the development and function of the ear is completely unknown.

D. Conservation and Development of the Vertebrate Ear

i. Anatomy and Physiology of the Vertebrate Inner Ear

Vestibular and auditory sensation are carried out by similar structures in humans and zebrafish with some notable alterations, as reviewed by Riley & Phillips (2003) (Fig. 2). In both species, vestibular sensation occurs in the utricle for detection of linear horizontal acceleration, and the semicircular canals which detect angular acceleration in different planes. In humans, another vestibular organ called the saccule is used for detection of vertical acceleration. The saccule is also present in zebrafish; however, in zebrafish the saccule is used for detection of vertical acceleration and for auditory sensation (Fig. 2). It works in combination with the swim bladder and a specialized sensory organ called the lagena. The swim bladder links to the saccule through three small bones called the Weberian ossicles (Bang, Sewell, & Malicki, 2001). The utricle, saccule and lagena possess luminal bodies composed of calcium carbonate and protein called otoliths which assist in sensation by increasing sensory cell activity through inertial and gravitational movement. Humans do not possess a lagena, but have a single organ for hearing called the cochlea (Fig. 2). Although fish do

not have a cochlea, the physiology underlying sensory cell function is highly conserved.

In both species, the vestibular and auditory organs described above rely upon sensory hair cells (Fig. 3) as receptors to sense vibrations created by acceleration or sound. Hair cells are found in sensory patches called cristae at the base of the semicircular canals, in the organ of Corti in the cochlea, and in maculae present in the utricle, saccule and lagena (Fig. 2), and are bathed in a high potassium fluid called endolymph. Hair cells possess a polarized apical surface with rows of stereocilia, which are actin-based, microvilli-like, and connected to one another by tip, horizontal, and ankle links (Fig. 3) (Nicolson, 2005). Rows of stereocilia increase in height in a staircase-like organization, and the tallest are connected by a kinocilial link to a single kinocilium, a true cilium with a microtubule-based core (Fig. 3) (Nicolson, 2005). Kinocilia are used to couple stereociliary bundles to an overlying gelatinous extracellular matrix that assists in the deflection of hair cells in sensory patches (Nicolson, 2005). In the semicircular canals this matrix is the cupula, in the cochlea it is the tectorial membrane, and in the utricle, saccule and lagena it is the otolithic membranes, which bind kinocilia to otoliths so that they can serve as additional inertial masses for stereociliary bundle deflection.

When the linked stereocilia are deflected in one direction by a vibrational disturbance to their overlying cupula, tectorial membrane, or otoliths, mechanically-gated potassium ion channels at the tips of the stereocilia are pulled open and potassium ions from the endolymph enter (Fig. 3). This

depolarizes the hair cell membrane and opens electrically-gated ion channels to allow calcium to enter the hair cell, which in turn succeeds in signaling for the release of neurotransmitter at the basal membrane (Fettiplace & Kim, 2014). At an associated synapse, the released neurotransmitter is responsible for starting an action potential that propagates along the vestibulocochlear nerve to the brain for processing.

Mechanotransduction of hair cell bundles relies on the structural integrity of its parts (Nicolson, 2005). In addition to stereocilial and kinocilial links, stereocilia bundles are stabilized by a dense actin meshwork known as the cuticular plate (Nicolson, 2005). The cuticular plate is located just below the apical surface of hair cells and connects with the actin-based cores of the stereocilia (Nicolson, 2005). Maintenance of the cuticular plate and its associated stereocilia is dependent on tip-link protein cadherin 23, myosin 6 (Kernan & Zuker, 1995; Seiler et al., 2004), and myosin 7a (Ernest et al., 2000; Sollner et al., 2004).

The hair cells of the zebrafish lateral line system are anatomically and physiologically similar to those of the inner ear, and can be used as a proxy in research because they are easier to access than inner ear hair cells (Mirkovic, Pylawka, & Hudspeth, 2012). Like the inner ear described above, the zebrafish lateral line consists of mechanosensory hair cells for sensation. These are grouped with support cells into organs called neuromasts which function to detect external vibrations close to the body for behaviors such as schooling, prey detection, and predator and obstacle avoidance (Coombs, Fay, & Janssen,

1989). Each neuromast of the lateral line consists of two equal-sized populations of hair cells oriented 180º relative to each other in order to respond to stimuli in either direction along the neuromast axis of sensitivity (Ghysen & Dambly-Chaudiere, 2007; Lopez-Schier et al., 2004). Mirkovic et al. (2012) demonstrated that neuromast hair cells and their centrosomes (during immature stages) undergo rotational rearrangement, and that this can occur twice as the neuromast develops to maturity.

ii. Development of the Zebrafish Ear

The development of the inner ear is highly conserved in all vertebrates, although the timings of proliferation and differentiation events vary somewhat between species (Haddon & Lewis, 1996). The result of these events are the three main cell types of the inner ear occurring together in a conserved relationship, those being hair cells, support cells and neurons (Riley & Phillips, 2003).

Development of the inner ear is well characterized in the zebrafish and is described in detail below (Fig. 4) (Haddon & Lewis, 1996; Whitfield et al., 2002). The ear is first initiated as a placode that forms on either side of the hindbrain from the posterior end of rhombomere 4 through rhombomere 6, which becomes visible by 16 hpf as the neural ectoderm thickens (Fig. 4) (Haddon & Lewis, 1996). Development begins with the specification of the tissue from the lateral edges of the hindbrain (Groves & Bronner-Fraser, 2000) and subjacent mesendoderm (Riley & Phillips, 2003). Otic placode induction is regulated

primarily by Fgf3 and Fgf8 signaling pathways, which in turn regulate other genes such as *sox9a*, *pax2a*, *pax2b*, and *pax8*, all of which are required for proper placode induction (Hans, Liu, & Westerfield, 2004; Liu et al., 2003). Patterning of the placode is believed to be controlled by signals from pharyngeal endoderm (Jacobson, 1963) and is hypothesized to be controlled by Fgf3 and Shh (Riley & Phillips, 2003).

At approximately 18 hpf, the placode cavitates to form a lumen (Fig. 4). The structure is termed the otic vesicle at this point (Haddon & Lewis, 1996), and consists of an epithelial sac containing hair cells (Sprague et al., 2006). Genesis of the otic vesicle requires interactions with adjacent tissues and incorporation of additional cells from the neural crest and mesoderm (Couly et al., 1993; Fritzsch et al., 1997; Noden, 1986). Patterning of the otic vesicle relies on Hedgehog signaling from underlying midline structures (Hammond et al., 2003). Of note is that mammals do not form the otic vesicle by cavitation, but by invagination to create a cup-like shape that later seals shut (Riley & Phillips, 2003); however, genes regulating the formation of the vesicle are highly conserved (Riley & Phillips, 2003).

The initial expansion of the otic vesicle lumen is closely followed in time by the appearance of a pair of hair cells at the anterior and posterior poles of the otic vesicle (Haddon & Lewis, 1996). These hair cells do not function in sensation until 23 hpf (Tanimoto, Ota, Inoue, & Oda, 2011); rather, their initial role is to bind otolith precursor particles at the tips of their kinocilia as nucleation sites for the

developing otoliths of the utricle and saccule (Fig. 4). Due to this specialized role, these kinocilia are referred to as tether cilia (green lines in Fig. 5).

Genesis of hair cells is regulated by hair cell fate determination factor Atoh1b, one role of which is to modify the action of the ciliogenic gene *foxj1b* to result in kinocilia differentiation (Yu et al., 2011). By 48 hpf there are approximately 10 - 20 hair cells per macula, and after 72 hpf the number of hair cells grows in each macula by about 15 cells per day until a final number of 50 to 60 hair cells is reached at maturity (Haddon & Lewis, 1996). The cristae are formed from 60 hpf to 72 hpf, and each contains about 20 hair cells at maturity (Haddon & Lewis, 1996).

Cilia are hair-like organelles that project from the apical surface of most vertebrate cell types (Fliegauf et al., 2007). They are composed of a microtubule core known as the axoneme, which is covered with plasma membrane continuous with that of the cell body (Fig. 6) (Satir & Christensen, 2007). Basal bodies, a pair of specialized centrioles, are required to position the axoneme and anchor it into the apical surface of its supporting cell (Ainsworth, 2007). Cilia exist in both immotile and motile forms (Fliegauf et al., 2007). Immotile cilia function in sensation of physical and biochemical extracellular signals (Satir & Christensen, 2007). Motile cilia use the motor protein dynein to bend along their length in order to move substances across epithelia, such as mucus in the respiratory tract and cerebrospinal fluid in the brain (Satir & Christensen, 2007). Cilia are assembled in quiescent cells after a mature centriole migrates and docks beneath the cell membrane (Ishikawa & Marshall, 2011). If a ciliated cell becomes mitotically

active, the cilium is reabsorbed by the cell preceding division (Quarmby & Parker, 2005).

Immotile and motile forms of monocilia extend from every epithelial cell of the otic vesicle upon the opening of its lumen (Fig. 7) (Stooke-Vaughan et al., 2012). The number of ciliated cells at this stage is approximately 100, and increases to approximately 225 by 24 hpf (Riley et al., 1997). Two cilia types which are critical for proper ear development include kinocilia, which were discussed above, and motile cilia. Large numbers of short motile cilia are initially present throughout the otic vesicle, but they decrease in length and disappear by 24 hpf (Yu et al., 2011). There are also motile cilia present on epithelial cells immediately surrounding the hair cells at the poles of the otic vesicle which persist past 24 hpf and are intermediate in length between the short cilia and the tether cilia of the otic vesicle.

By 19.5 hpf two otoliths appear at the poles and become attached to tether cilia by 20 hpf (Riley & Phillips, 2003), a process which is critically dependent on motile cilia to circulate fluid which transports otolith precursor particles within the otic vesicle lumen (Riley et al., 1997). Additionally, throughout these time points, neuroblasts delaminate from the otic vesicle and differentiate into neurons that will comprise the 8th cranial nerve (Haddon & Lewis, 1996).

At 45 hpf, epithelial projections grow into the lumen and there fuse at 55 hpf to form the hubs around which three semicircular canals will develop (Riley & Phillips, 2003) (Fig. 2). This process of morphological formation requires the gene *ugdh* which produces one of the subunit building blocks of hyaluronic acid

(Walsh & Stainier, 2001), and its putative regulator gene *dfna5*, a known human deafness gene (Busch-Nentwich et al., 2004; Gregan et al., 2003). These are members of a collection of genes shown to be necessary for semicircular canal formation, which also includes *dlx5, hmx2, hmx3 and fgf10* (as reviewed by Chang et al., 2004). Multiple *bmp* genes cooperate to regulate development of the semicircular canals and sensory cristae as well (Riley & Phillips, 2003).

The ear is functional by 96 hpf in zebrafish larvae, when the acoustic startle response, and an ability to orientate relative to gravity can be observed (Kimmel, Patterson, & Kimmel, 1974). Later in larval development, the main chamber of the otic vesicle subdivides into the utricle, saccule and lagena, a third otolith forms in the lagena, and the anterior and posterior macula mature into four distinct macula (Platt, 1993). These are the utricular, saccular, and lagenar macula discussed above, and the macula neglecta (Fig. 2), which senses low frequency vibration (Corwin, 1983). Genes found to be responsible for otic vesicle maturation and compartmentalization include *pax2*, *gata3*, *dlx3*, and *bmp4* (Fekete & Wu, 2002; Fritzsch & Beisel, 2001; Torres & Giraldez, 1998). Also, it should be noted that *myh9* is included in the category of genes already identified here that are known to be expressed in or adjacent to the otic vesicle (Mhatre et al., 2006).

iii. Otoliths

Otoliths, also known as otoconia or ear stones, are masses of minerals and proteins that act as inertial loads in the mature ear to assist with the

deflection of hair cell stereocilia (Fig. 2). During development in zebrafish, otoliths are crystalized from precursor particles that are emitted by epithelial cells into the otic vesicle lumen beginning at 18.5 hpf and continuing to 24 hpf (Riley et al., 1997) in what is thought to be an apocrine process (Pisam et al., 2002). These precursor particles attach to tether cilia around 20 hpf and continue agglomeration at the ends of these cilia until ovoid masses are formed at the anterior and posterior poles of the otic vesicle (Figs. 4 and 5) (Riley & Phillips, 2003).

Otoliths grow from particles in a characteristic manner. As reviewed by Pisam et al. (2002), particles are initially arranged in parallel arrays which are then combined into pseudocrystalloid structures. These are then joined in concentric arrays called spherules, which aggregate into globules, and then combine into a roughly spherical otolith by 30 hpf. The otolith grows further in size and changes in shape by 50 hpf to have a flattened epithelium-facing hemisphere and a rounded hemisphere, and consists of an internal nucleus structure surrounded by two concentric layers of matrix (Pisam et al., 2002). This matrix includes glycoproteins, proteoglycans, and collagens, as well as calcium carbonate in aragonite form which comprises 90–95% of the otolith (Pisam et al., 2002). Several genes have been shown to be necessary for the process of otolith formation, including *otopetrin 1* and *starmaker* (Sollner et al., 2003). An otolith precursor-binding factor was hypothesized by Riley et al. (1997) that is responsible for localizing and adhering otolith particles to tether cilia, and other

research has supported a role for such a factor, although it has never been discovered (Stooke-Vaughan et al., 2012).

Otolith formation is also dependent on motile cilia in the otic vesicle to circulate fluid which transports otolith precursor particles (Riley et al., 1997) and keeps the otolith in a constant state of motion at the end of its tethers (Wu et al., 2011) (Fig. 7). Specifically, motile cilia are implicated in transporting precursor particles toward tether cilia to account for otolith number, position, and size (Colantonio et al., 2009), and in stirring the fluid at the otolith formation region of the otic vesicle to account for the flat base of the otolith (Wu et al., 2011).

The shape and size of otoliths is believed to be crucial for sensory function (Nicolson, 2005; Sollner et al., 2003). The two originally pseudo-spherical otoliths differ in shape and size once fully developed (Haddon & Lewis, 1996). The posterior otolith retains a somewhat spherical shape and measures 55 μm in diameter. The anterior otolith is smaller and discoid in shape, and measures about 25 μm in dorso-ventral thickness and 45 μm in diameter. It has been found that otolith size plays a critical role in acoustic sensory transduction, and growth of the otolith is tightly regulated during development so that it assumes an appropriate size for acoustic sensory transduction (Inoue, Tanimoto, & Oda, 2013). Shape may also be important for otolith function. In the zebrafish, this shape is aspherical, with a flat bottom and mushroom-shaped top (Wu et al., 2011). Wu et al. (2011) hypothesize that the flat-bottomed shape of the otolith allows orthogonal cilia implantation, allowing maximal sensitivity of stereocilia bundles to linear fluid displacements (Karavitaki & Corey, 2010; Wu et al., 2011).

iv. Cilia

Several genes have been identified that are necessary for ciliary motility. *Foxj1b* is a regulator of ciliary motility that is first expressed at 10 hpf in the nascent otic placode (Yu et al., 2011). Once the otic placode is formed at 16 hpf, until the time point of 22 hpf, its expression gradually becomes spatially restricted to the poles of the otic vesicle (Yu et al., 2011). This expression pattern is thought to mirror the locations of motile cilia through these time points (Riley et al., 1997; Yu et al., 2011). Other genes required for ciliary motility are the dynein regulatory complex genes *gas8* (Colantonio et al., 2009) and *dnaaf1* (Stooke-Vaughan et al., 2012).

The proportion of otic vesicle cilia that are motile throughout development is disputed in current literature. According to Stooke-Vaughan et al. (2012), the number of cells having motile cilia remains constant over these developmental stages with a number of approximately 5 for wild-type AB zebrafish, and these cilia are to be found at an anterior and a posterior pole as well as along the medial wall of the otic vesicle. Additionally, Stooke-Vaughan and colleagues found that tether cilia are immotile. Colantonio et al. (2009) argued that tether cilia are the only motile cilia present in the otic vesicle. Riley et al. (1997) predicted that large numbers of short cilia in the otic vesicle would be motile and hair cell kinocilia would be immotile, and this view was substantiated by the experimental evidence of Yu et al. (2011).

In polarized epithelia, the correct orientation of the cilia and their basal bodies is determined by translational and rotational polarity. As described by Mirzadeh et al. (2010), translational polarity refers to the position of basal bodies near the apical surface of the cell, and rotational polarity describes the angle of individual basal bodies with respect to their long axis (Fig. 6). Either of these two polarities can affect the orientation and tilt of the long axis of a cilium (Mirzadeh et al., 2010). This positional information is critical for the correct orientation of motile cilia and their basal bodies in order to produce ciliary movement necessary to achieve normal fluid flow within the otic vesicle (Marshall & Kintner, 2008); however, the cellular mechanisms responsible for setting up and maintaining correct ciliary polarity in the otic vesicle are not completely understood.

Movement of the motile cilia in the otic vesicle is rotary (Stooke-Vaughan et al., 2012). If the long axis of a cilium were positioned perpendicularly to the cell membrane, the resultant fluid flow produced by the cilium would be a vortex. The effect of multiple cilia beating in this manner, in a consistent direction, within a fluid-filled vesicle, would be a circular flow around the epithelium (Nonaka et al., 2005). This is contrary to what is found in the zebrafish otic and Kupffer's vesicles, where a linear flow exists instead (Essner et al., 2005; Wu et al., 2011). Linear flow is achieved by tilting the cilium so that its tip passes close to the apical membrane in one part of its elliptical path, or drags along it to produce a D-shaped path if the tilt angle is sufficiently obtuse (Nonaka et al., 2005). Because fluid near a solid surface does not move as readily as fluid far from a

surface (this phenomenon is termed the no-slip boundary condition), the cilium produces less fluid flow in the direction of its path directed away from the surface and more force in the opposing direction (Brokaw, 2005). The result of many motile cilia moving in the same direction with the same direction of tilt is continuous fluid flow in one direction (Brokaw, 2005).

The Role of *Myh9* in the Ear

We conducted *myh9* knockdown experiments in zebrafish and found abnormal number of otoliths at 36 hpf. Based on this finding, we hypothesize that there is a defect in the development or function of cilia in the developing ear of zebrafish with *myh9* knockdown. We further hypothesize that *myh9* is required for ciliary orientation or motility, which may impact sensory processes, hair cell structural integrity, cell signaling in the ear, or mechanical ciliary function to account for deafness symptoms when the gene is mutated. Using the zebrafish as a model, we investigated the role of *myh9* in ear development and function as a first step toward understanding the mechanisms involved in *MYH9*-related disease, which is the purpose of this thesis.

	DNA	Protein
myh9	79.3%	83.3%
myh9a	77%	77%

Table 1: Zebrafish homology with human *MYH9*. Data indicates the percentage of matching sequence identity between the DNA of the zebrafish genes *myh9* or *myh9a* and the human gene *MYH9*, as well as the percentage of matching sequence identity in the protein products of these genes. *myh9a* is an ohnolog to *myh9*, and is not present in humans. (Flicek et al., 2014).

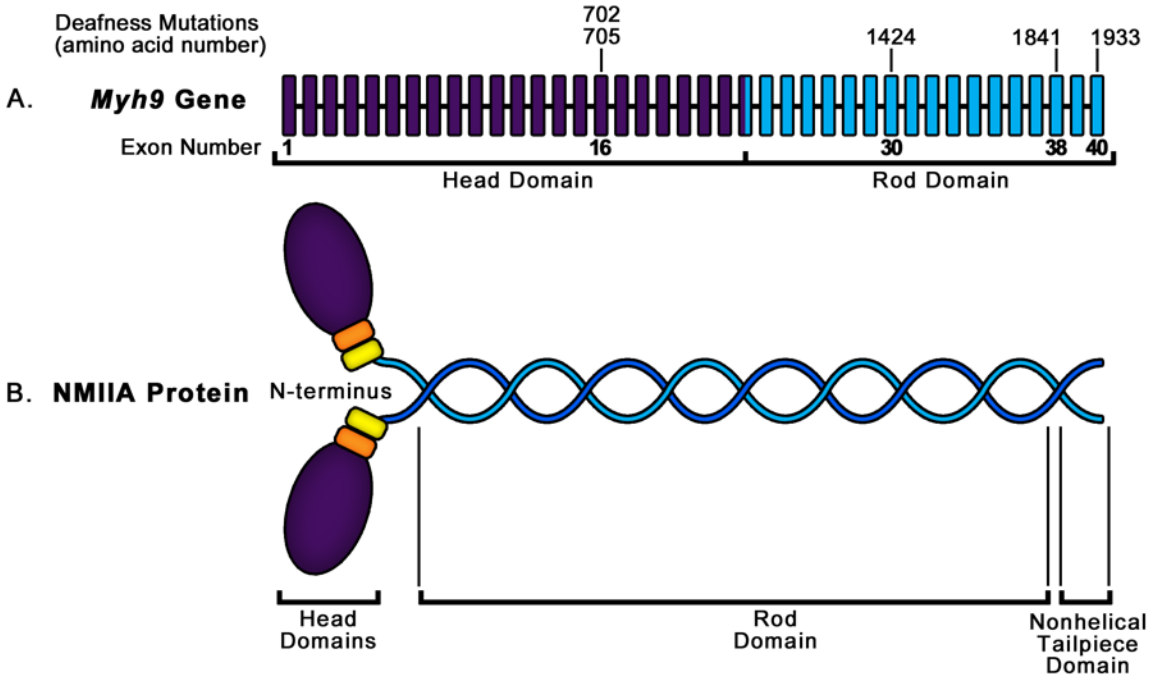

Fig. 1: The *myh9* gene and its protein product, non-muscle myosin IIA. (A) The *myh9* gene is comprised of 40 exons; those coding for the head domain are shown in purple, and those coding for the rod and tailpiece domains are shown in blue. Mutations causing deafness are present at amino acids 702, 705, 1424, 1841 and 1933. (B) The NMIIA protein consists of a dimer made up of a head, neck, rod, and nonhelical tailpiece domain. The myosin regulatory and essential light chains are bound to the neck domain, shown in yellow and orange, respectively.

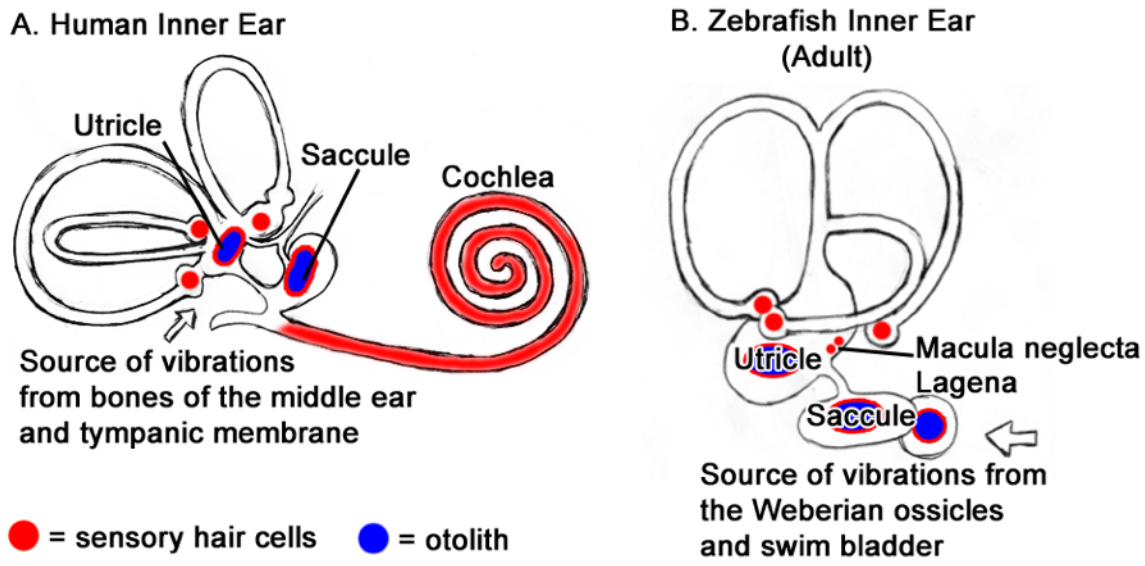

Fig. 2: Inner ear structure is highly conserved between humans and zebrafish. (A) Human inner ear. (B) Adult zebrafish inner ear. Locations of hair cells are indicated in red; locations of otoliths are indicated in blue. Auditory sensation is carried out by the cochlea in humans and the saccule and lagena in zebrafish. Humans and zebrafish use the macular organs of the utricle and saccule to detect linear acceleration as part of their vestibular systems.

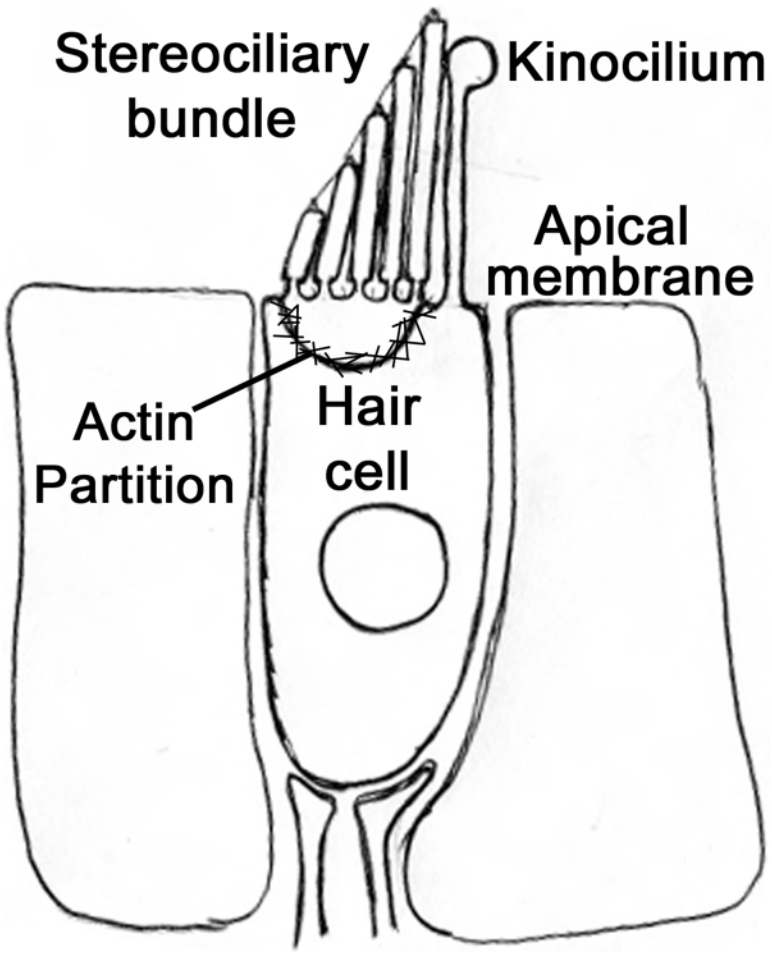

Fig. 3: Structure of a hair cell. Hair cells are sensory cells of the auditory and vestibular systems in humans and zebrafish, as well as the lateral line system in zebrafish. The cells possess a staircase-like arrangement of actin-based microvilli on their apical surface as well as a microtubule-based kinocilium used to detect motion in extracellular fluid. Hair cells are positioned in close proximity to support cells that assist their function.

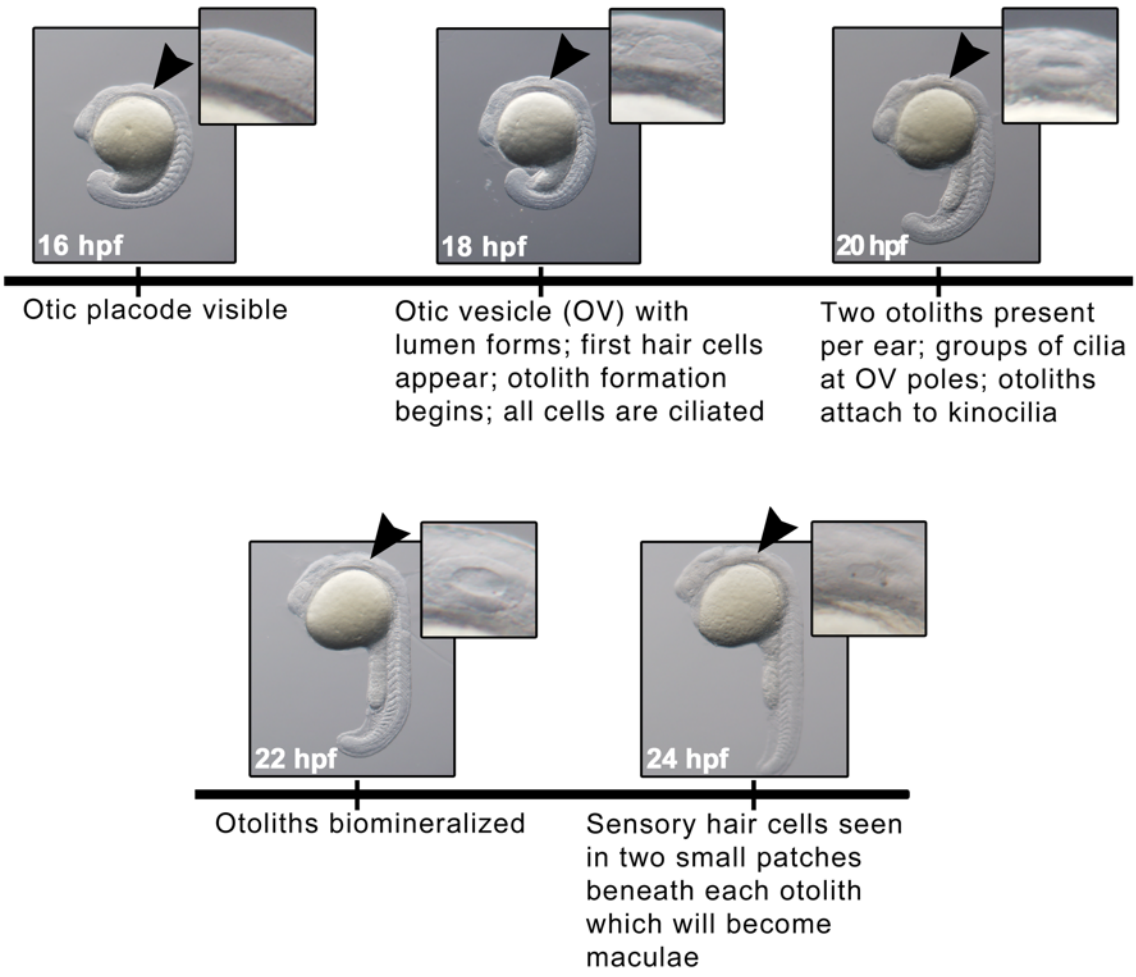

Fig. 4: Zebrafish ear development between 16 and 24 hpf. Black arrowheads indicate the location of the developing ear; inset boxes show a higher magnification image of the developing ear. Otoliths are visible by brightfield imaging at otic vesicle poles by 22 hpf. Anterior is to the left in all images.

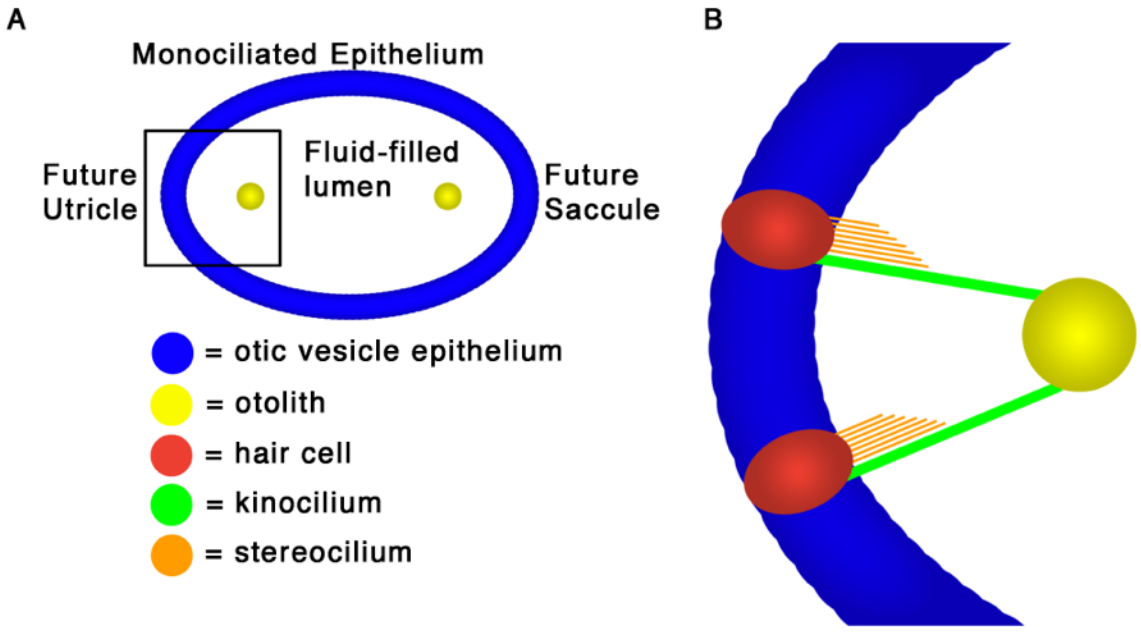

Fig. 5: Structures of the zebrafish otic vesicle. (A) Diagram of the embryonic zebrafish otic vesicle at 24 hpf. (B) Magnification of the boxed region of A showing detailed anatomy of one pole of the otic vesicle indicating hair cells, hair cell cilia, and otolith location.

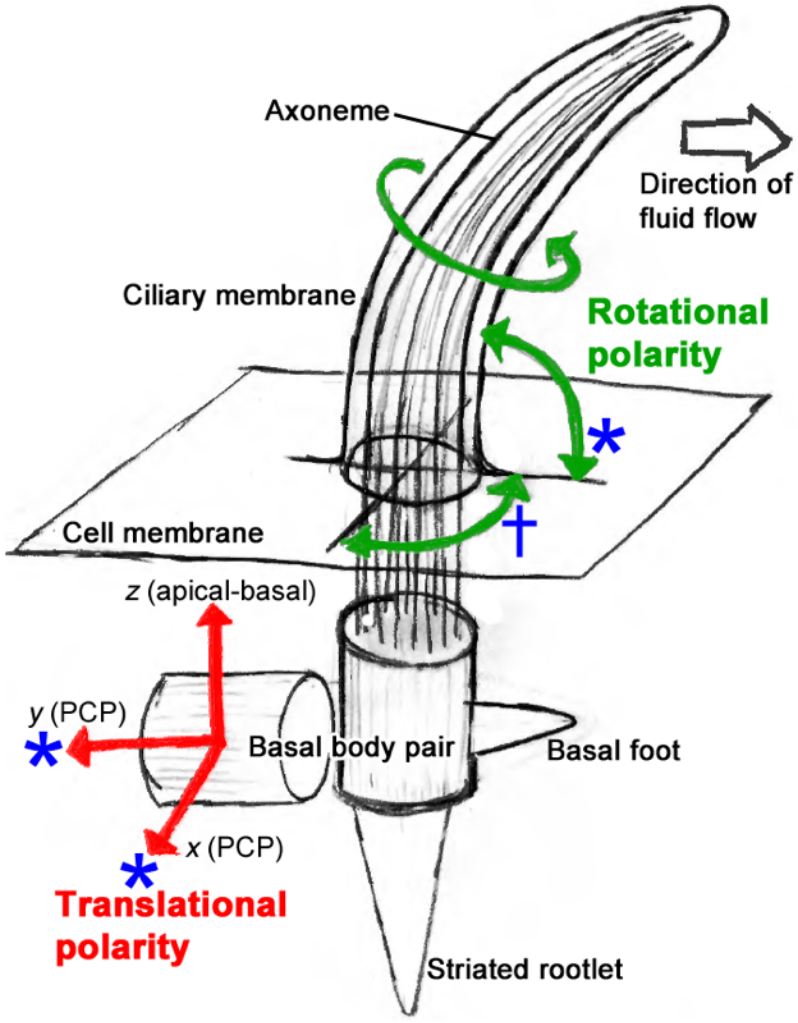

Fig. 6: Cilia structure and polarity. Cilia anatomy is labeled as indicated. Six values describe the orientation of a cilium. The x, y, and z Cartesian coordinates describe translational polarity (shown in red), and three angles describe rotational polarity (shown in green). The blue asterisks indicate the polarity values that affect ciliary tilt. The blue cross indicates perpendicular rotation.

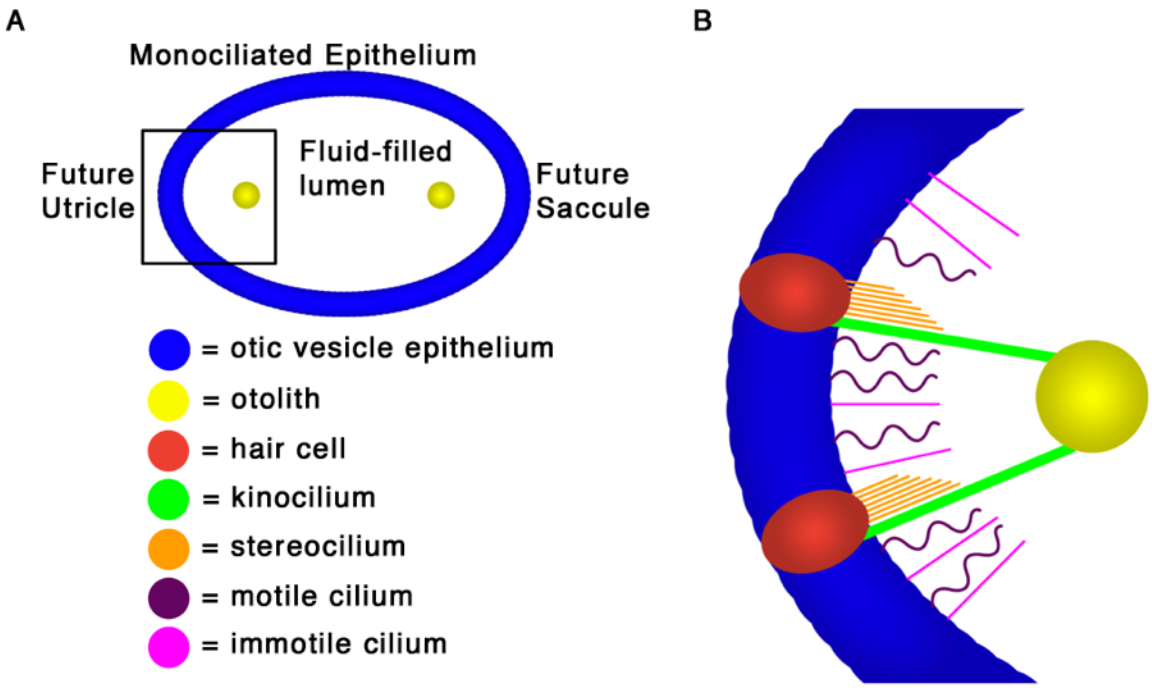

Fig. 7: Structures of the zebrafish otic vesicle. (A) Diagram of the embryonic zebrafish otic vesicle at 24 hpf. (B) Magnification of the boxed region of A showing detailed anatomy of one pole of the otic vesicle, including epithelial cell motile and immotile cilia.

Chapter 2: Characterization of a Non-Muscle Myosin IIA-Dependent Otolith Phenotype

Introduction

MYH9 has been identified as a gene that can lead to human deafness when mutated. This symptom is found in two categories of disease. The first is a condition named autosomal dominant nonsyndromic deafness 17 (DFNA17), which results in an onset of high frequency sensorineural hearing loss beginning near ten years of age that degenerates to severe deafness at all frequencies near age thirty (Lalwani et al., 1999). The other category of disease consists of four similar disorders collectively labeled *MYH9*-related diseases, which share the hematological symptoms of abnormal platelets and leukocytes, and include deafness as a variably-occurring symptom (Mhatre et al., 2007).

MYH9 codes for the protein non-muscle myosin IIA (NMIIA), which is one isoform of the more general class of myosins called non-muscle myosin II (NMII). This class also includes the isoforms non-muscle myosin IIB (NMIIB) and non-muscle myosin IIC (NMIIC). The human *MYH9* gene consists of 40 exons (Kunishima & Saito, 2010) and the mutations that most consistently lead to the deafness phenotype occur in exons coding for the catalytic head domain of the NMIIA protein, where ATP is hydrolyzed to create a conformational change in the protein that allows it to move along actin (Huang et al., 2013).

Myh9 is expressed in both the apical and basal membranes of mouse otic vesicle epithelial cells from the beginning of the vesicle formation at embryonic day 10.5 (Mhatre et al., 2004). Continued expression is present throughout mouse development to maturity within several tissues of the cochlea, including

the cochlear duct and hair cells (Mhatre et al., 2006). Also, Gutzman et al. (in review) demonstrated in the zebrafish that *myh9* is expressed throughout the embryo during the 16 - 24 hpf developmental period that is critical for ear formation (Haddon & Lewis, 1996).

We hypothesized that NMIIA is required for vertebrate ear development and function. In order to test this hypothesis we used the zebrafish as a model system. Zebrafish provide a useful model for examining the molecular basis for how *myh9* mutations cause deafness for several reasons. There is a high degree of conservation between the anatomy and physiology of human and zebrafish inner ear structures (Fig. 2) (Thomas et al., 2013). There is also high sequence homology between the human and zebrafish *MYH9* genes (Table 1). Lastly, zebrafish embryos are transparent in early development, mature externally, and are born in large clutches, making them ideal for studying the development and function of the ear.

We conducted our studies during the ages of 16 hpf to 24 hpf in the zebrafish. During this time frame, the otic placode is formed and cavitates, the lumen of the otic vesicle expands, hair cell pairs develop at anterior and posterior poles of the lumen with specialized tether cilia, motile cilia are generated, and two otoliths are formed (Fig. 4) (Haddon & Lewis, 1996; Riley et al., 1997). Otoliths are of keen importance to hearing in zebrafish due to their roles as inertial masses for deflection of stereociliary bundles in auditory sensory cells (Nicolson, 2005). Within the indicated eight hour period of ear development, the stages of 19 to 24 hpf are especially critical for otolith formation (Riley et al.,

1997). The rate of growth of otoliths is most rapid during these stages, and its normal progression is reliant on a biological flow in the otic vesicle lumen perpetuated by beating cilia that disappear by 24 hpf (Colantonio et al., 2009; Riley et al., 1997).

We tested the role of *myh9* in the development and function of the zebrafish ear through a series of loss-of-function experiments. These were directed against the more general class of NMII proteins, as well as NMIIA. We found that NMII, and specifically NMIIA, loss-of-function resulted in the development of an abnormal number of otoliths in the zebrafish otic vesicle. These experiments indicate the importance of NMIIA in development of the ear and suggest that the zebrafish will be a useful model to uncover how *myh9* mutations lead to deafness in *MYH9*-related diseases.

Materials and Methods

Animals

For all studies, we used wild-type AB zebrafish. Embryonic stages are given as hours post fertilization (hpf). Standard procedures were used for zebrafish maintenance, husbandry and staging (Kimmel et al., 1995).

Morpholino (MO) injections

Splice-site blocking morpholinos (Gene Tools) were dissolved in water and injected into one- to two-cell stage embryos in combination with membrane

targeting GFP (mGFP). Morpholinos and their sequences, targeted splice sites, and concentrations used are as follows:

• *myh9* MO: 5'- ATGTCTGAAACAGTCGTTTACAAGC-3'; targets the zebrafish *myh9* gene at EXON6-intron6 boundary. It was used at 3 ng/µl for all experiments. The *myh9* sequence information is based on zebrafish Ensembl transcript ENSDART00000137105.

• *myh9a* MO: 5'-AGCAAGAGAGACTTACAAATCGAGA-3'; targets the zebrafish *myh9a* gene at intron1-EXON2 boundary. It was used at 4 ng/µl for all experiments. The *myh9a* sequence information is based on zebrafish Ensembl transcript ENSDART00000149823.

• standard control MO: 5′-CCTCTTACCTCAGTTACAATTTATA-3′; has no target. It was used at a concentration matching that of each experimental MO (*myh9* MO or *myh9a* MO).

•*p53* MO: GCGCCATTGCTTTTGCAAGAATTG-3'; targets the zebrafish *p53* gene. It was only used in conjunction with *myh9* knock down experiments (*myh9* MO and control MO) at an equal concentration to the test morpholino (Robu et al., 2007).

Blebbistatin treatment

16 hpf embryos were treated with 50 mM blebbistatin in 0.1% DMSO (Sigma-Aldrich, B0560) or 0.1% DMSO (Fisher Scientific, BP231-100) as control in E3 medium (5 mM NaCl, 0.17 mM KCl, 0.33 mM $CaCl_2$, 0.33 mM $MgSO_6$) for three hours, then washed 3X in E3 medium. Embryos were then allowed to develop

until 36 hpf for analysis of otolith phenotypes. For embryo rotation experiments, incubated embryos were placed in a six-well plate with 3 mL of 50 mM blebbistatin or 0.1% DMSO E3 medium, and the plate was placed on a rotator (Barnstead) at 28ºC for three hours and gently rotated to slightly move the embryos during the incubation.

Immunohistochemistry

Blebbistatin- or DMSO-treated embryos were raised to 24 hpf in E3 medium at 28ºC, then were fixed in 4% paraformaldehyde for 2 h at room temperature or overnight at 4°C. Embryos were blocked in 10% goat serum and 0.1% BSA in PBT overnight, incubated overnight in primary antibody (anti-phosphorylated histone H3, Millipore, 06-570, 1:800), then incubated overnight in secondary antibody (goat anti-rabbit IgG conjugated with Alexa Fluor 488, Invitrogen, A11008, 1:500), in combination with propidium iodide (Invitrogen, P3566, 1:1000). Embryos were mounted in glycerol and imaged using a Nikon CS2 laser-scanning confocal microscope. Images were analyzed with Nikon Elements software and Photoshop (Adobe).

PH3 Analysis

Confocal stacks of the otic vesicle from embryos immunostained for phosphorylated histone H3 to label nuclei of proliferative cells and stained with propidium iodide to label all nuclei were merged into a maximum intensity

projection using Nikon Elements software. Proliferative cells were counted, averaged, and compared between control and *myh9* morphant embryos.

Otolith Phenotype Analysis

Embryos were placed in a 90 mm petri dish containing E3 medium and anesthetized using tricaine mesylate (Sigma-Aldrich, E10521, 4%). Embryos were positioned laterally and otoliths were counted in both developing ears using oblique illumination on an Olympus SZX12 stereomicroscope. Embryos were tilted to ensure superficial otoliths were not obscuring deeper otoliths within the lumen of the otic vesicle. Only otoliths completely free from contact with other otoliths were counted; otoliths contacting one another were counted as a single otolith.

Imaging

All live confocal imaging was conducted as previously described (Graeden & Sive, 2009) using a Nikon CS2 scanning confocal and Nikon Elements software. Brightfield imaging was conducted using an Olympus SZX12 stereomicroscope with an Olympus DP72 camera. All images were processed using Nikon Elements software or Photoshop (Adobe).

Statistical Analysis

Significance testing of differences in numbers of proliferative cells between control and morphant embryos was conducted using the Mann-Whitney *U* test at

a significance level of 0.05. Significance testing of differences in numbers of otoliths between the ears of control and morphant embryos was conducted using Fisher's exact test of independence for 2 x 2 tables at a significance level of 0.0001.

Results

Myosin II is required for normal otolith formation in the developing ear.

To begin our investigation into the role of *myh9* in deafness, we focused our experiments on the entire class of NMII proteins by employing a myosin II inhibitor. NMII carries out a variety of intracellular functions including cell migration, cell division, and cell shape changes through interaction with the actin cytoskeleton (Lo et al., 2004; Saitoh et al., 2001; Svitkina et al., 1997). The rationale for beginning experiments with the broader category of NMII as opposed to NMIIA is that the alternate NMII isoforms, NMIIB and NMIIC, may compensate for reduced or ineffective NMIIA in tissues susceptible to variable disease symptoms in *MYH9*-related disease, such as the kidney, eye and inner ear (Heath et al., 2001). By inhibiting all isoforms, we were able to observe the full effect of any ear-related phenotype resulting from a loss-of-function of NMII.

To conduct loss-of-function experiments on NMII, we used the myosin II inhibitor blebbistatin. Myosin II proteins are actin contractile motors that function by first binding ATP at the head domain of the myosin protein, which causes its dissociation from actin (Xiao et al., 2003). Next, the bound ATP is hydrolyzed,

leading to extension of the myosin head domain as a conformational change to the protein. The head domain then binds actin once more, which causes release of a free phosphate. ADP is released next, which initiates another conformational change in the myosin head. This second change moves myosin relative to actin, and provides the force responsible for myosin's contraction. Blebbistatin inhibits this contraction by preferentially binding to the ATPase intermediate with ADP and phosphate bound at the active site, where it slows down the release of the free phosphate (Kovacs et al., 2004).

To test the hypothesis that myosin II is required for normal development of the zebrafish ear, wild type embryos were raised to 16 hpf in E3 medium, then exposed to 50 mM blebbistatin, or 0.1% DMSO as a control. After incubation for three hours in blebbistatin or DMSO, the embryos were washed in E3 medium and allowed to develop to 36 hpf. During this 19 to 36 hpf time period, the ears of embryos were frequently analyzed for any defects by oblique microscopy. We discovered that embryos treated with blebbistatin developed an abnormal number of otoliths as compared with DMSO-treated control embryos (Fig. 8A - B'). Observed abnormal numbers of otoliths included one, three or four otoliths, with three otoliths being the most common. Otolith numbers were then quantified at 36 hpf (Fig. 8C). To accurately count the otoliths, embryos were anesthetized and positioned laterally along the bottom of a petri dish. The otoliths counted were observed as single entities in the otic vesicle lumen and were free from any contact with other otoliths. By varying oblique illumination on the microscope and slightly rocking the embryo, we were able to ensure that all otoliths were counted,

avoiding the possibility of otoliths being hidden from view either due to the positioning of the embryo, or due to a more superficial otolith preventing detection of a deeper one. Both ears were counted in this way and treated as independent data points. We demonstrated that the inhibition of NMII resulted in the appearance of an abnormal number of otoliths in 28.2% of the ears analyzed, with no abnormalities found in controls (Fig. 8C).

Stooke-Vaughan et al. (2012) tested the hypothesis that otolith defects were exacerbated by diminished muscular activity in zebrafish embryos possessing mutations resulting in a motility defect. Stooke-Vaughan and colleagues were able to partially rescue the otolith defects in these mutants by mechanically rolling immobile embryos during development (Stooke-Vaughan et al., 2012).

Since blebbistatin is a myosin II inhibitor, it is known to also inhibit muscle activity (Kovacs et al., 2004); therefore, we performed additional experiments in which embryos were gently rotated during the period of blebbistatin treatment to determine whether mobility of the embryo was a contributing factor to the otolith phenotype (Fig. 8C). We found that rotation did not rescue the otolith phenotype. Approximately 36 percent of ears counted had an abnormal otolith number, consistent with our non-rotational results (Fig. 8C). Together our data suggests that NMII is necessary for proper otolith development in the otic vesicle.

Myosin II and cell division in the developing ear.

Since we determined that NMII loss-of-function results in abnormal otolith number, we wanted to determine if the otolith phenotype was the result of abnormal cell division following blebbistatin treatment. To test this, we employed immunohistochemistry and confocal microscopy to quantify nuclei of proliferative cells during zebrafish otic vesicle development. Developing embryos were treated with DMSO or blebbistatin, as described above, and fixed at 24 hpf. We stained embryos with propidium iodide to label all nuclei and immunostained with anti-phosphorylated histone H3, an antibody raised against phosphorylated serine 10 present during the S phase of cell division, which marks diving nuclei (Figs. 9A - F). We counted only proliferative cells in each otic vesicle and compared between treatments. We found that the blebbistatin treatment used for inhibition of NMII, which resulted in abnormal otolith number, did not alter normal cell proliferation (Fig. 9G). These data suggest that the role of NMII in regulating otolith number is not dependent on its function in cell division.

NMIIA is required for normal otolith formation in the developing ear.

While there are three genes coding for isoforms of NMII, only mutations in the *MYH9* gene leads to onset of *MYH9*-related diseases. Therefore, after studying the phenotypic effects of NMII inhibition using blebbistatin, we focused our studies on the specific loss-of-function of NMIIA. In order to specifically knock down NMIIA we used injection of antisense morpholino oligonucleotides. We designed splice site-blocking morpholinos targeting *myh9* as well as *myh9a,* an

ohnolog to *myh9* found in zebrafish, but not present in humans. Following morpholino injection at the one- to two-cell stage, embryos were raised to 36 hpf and assayed for otolith number. Phenotypes of *myh9* and *myh9a* morphants were compared to embryos injected with a control morpholino at an equal concentration (Fig. 10). We found that approximately 45 percent of *myh9* knockdown embryos had an abnormal number of otoliths, versus approximately 3 percent of controls (Fig. 10C). Knockdown of *myh9a* did not affect otolith number, indicating that *myh9a* is not required for correct otolith formation (Fig. 10D). Effectiveness of each morpholino was confirmed by RT-PCR (Gutzman et al., in review). Together these results indicate that *myh9*, but not *myh9a,* is required for normal otolith formation in the developing zebrafish.

Discussion

NMIIA is required for normal otolith formation in the developing ear.

We have demonstrated that NMII is required for normal development of otoliths by inhibiting its function with blebbistatin (Fig. 8). We have further demonstrated that an isoform of NMII, and the product of the *myh9* gene, NMIIA, is specifically required for normal otolith development using a second loss-of-function tool, a splice-blocking morpholino (Fig. 10). Together these two experiments support our main hypothesis that *myh9* is required for zebrafish ear development. Furthermore, these results support the use of the zebrafish as a model system to understand how mutations found in the human *MYH9* gene can result in deafness as a variable symptom of *MYH9*-related disease.

The mechanism for how *myh9* influences otolith formation is unknown. We hypothesize that a defect exists in the motility of cilia in the developing zebrafish ear with *myh9* loss-of-function because normal otolith development is affected by fluid currents generated in the otic vesicle by beating cilia (Stooke-Vaughan et al., 2012). Experiments have shown that defects in motile cilia can cause abnormal otolith number, size, and position (Colantonio et al., 2009).

Myosin II and cell division in the developing ear.

The number of ciliated cells increases in the zebrafish otic vesicle epithelium from approximately 100 at 19 hpf to approximately 250 by 24 hpf (Riley et al., 1997). As previously stated, NMII has a role in genesis of new cells by providing a contractile force necessary to separate dividing daughter cells during cytokinesis (Barua et al., 2014). Therefore, we inhibited NMII to determine whether or not, at this concentration of blebbistatin, cell proliferation was disrupted and therefore might have some effect on otolith number.

Our data did not demonstrate any significant difference in the number of proliferative cells at 24 hpf with NMII inhibition (Fig. 9), suggesting that the role for NMII in otolith formation is not dependent on regulation of cell proliferation. There are still several questions that might be answered by further experiments centered on cell proliferation in the otic vesicle. Is there a change in proliferation in the developing ear earlier or later in development that might affect otolith formation? Are the total number of cells consistent between the control-treated embryos and those treated with the myosin inhibitor? Finally, does the cell

division rate vary between the different cell types of the otic vesicle? Such a change may imply a requirement for NMII in specific cell populations within the otic vesicle.

Hypothesized role for *myh9* and otolith formation.

We conclude that NMIIA is required for proper ear development, based on the phenotype we discovered of an abnormal otolith number in *myh9* loss-of-function embryos. We also conclude that this otolith phenotype is not due to abnormal cell proliferation in the otic vesicle. These findings led us to hypothesize that the role for *myh9* in otolith formation is through regulation of motile cilia of the otic vesicle. Motile cilia are responsible for generating fluid forces that distribute otolith precursor particles within the lumen. For example, Stooke-Vaughan et al. (2012) showed that in zebrafish embryos with mutations in the axoneme assembly gene *lrrc50* which is required for ciliary motility, approximately 25% of ears counted had an abnormal number of otoliths. Similarly, Colantonio et al. (2009) found that knockdown of another gene required for normal ciliary motility, the dynein regulatory gene *gas8,* had the result of approximately 70% of ears with an abnormal number of otoliths (Colantonio et al., 2009). Finally, Yu et al. (2011) demonstrated irregularities in otolith formation due to the knockdown of *foxj1b*, a gene coding for a transcription factor regulating motile cilia which is expressed in the otic vesicle (Aamar & Dawid, 2010; Tian et al., 2009; Yu et al., 2008). Further work must be undertaken to

study the form and function of these motile cilia of the otic vesicle, and this is the focus of Chapter 3.

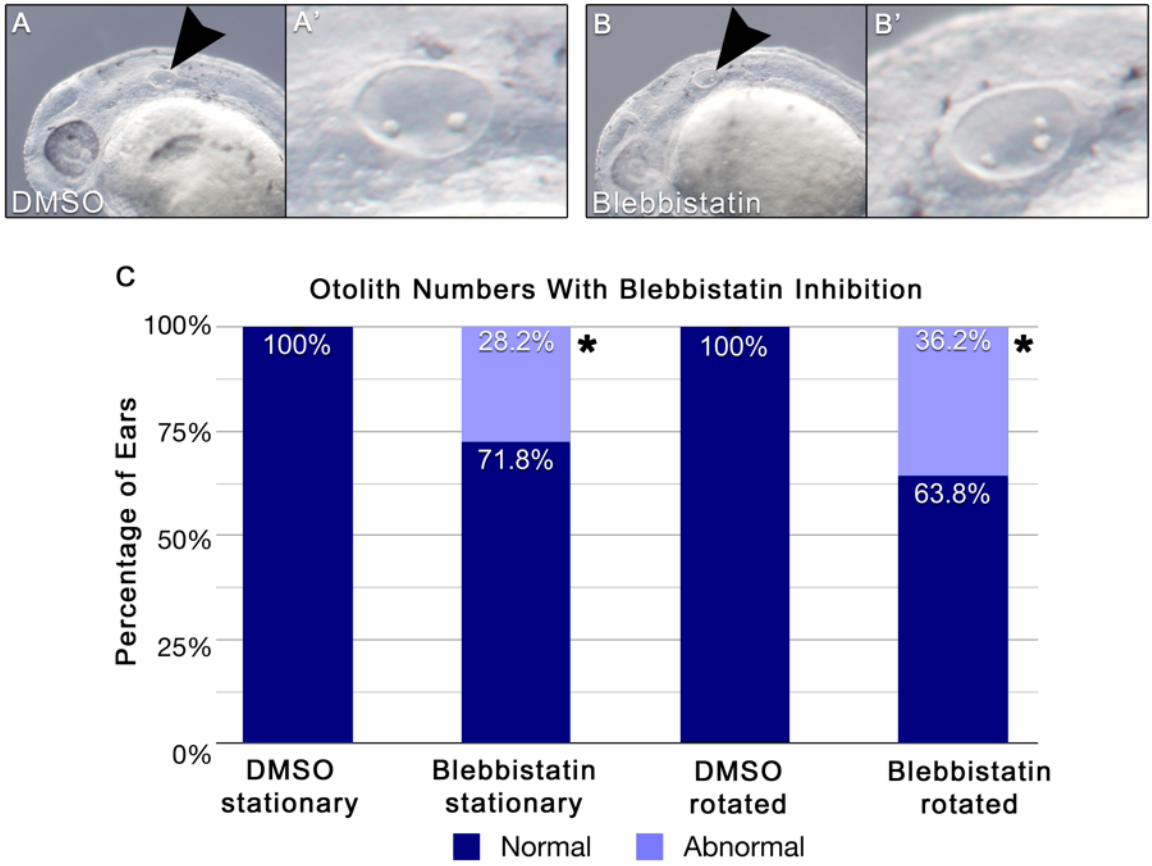

Fig. 8: Myosin II is required for normal otolith formation in the developing ear. 16 hpf embryos were treated with 50 mM blebbistatin or DMSO control for three hours. Embryos were then washed and otoliths were analyzed at 36 hpf. (A - B) Black arrowheads indicate the developing ear. (A) 36 hpf DMSO-treated embryo displaying normal otolith number. (A') Higher magnification of the ear from image A. (B) 36 hpf blebbistatin-treated embryo. (B') Higher magnification of the ear from image B. White arrowhead shows the third otolith. (C) Embryos were imaged and otoliths were counted at 36 hpf. Graph is of the percentage of normal and abnormal numbers of otoliths per ear when embryos were stationary or gently rotated during drug treatment. Asterisks indicate significance as tested using Fisher's exact test of independence for 2 x 2 tables at a significance level of 0.0001. DMSO stationary: n=286; blebbistatin stationary: n=266; DMSO rotated: n=144; blebbistatin rotated: n=149.

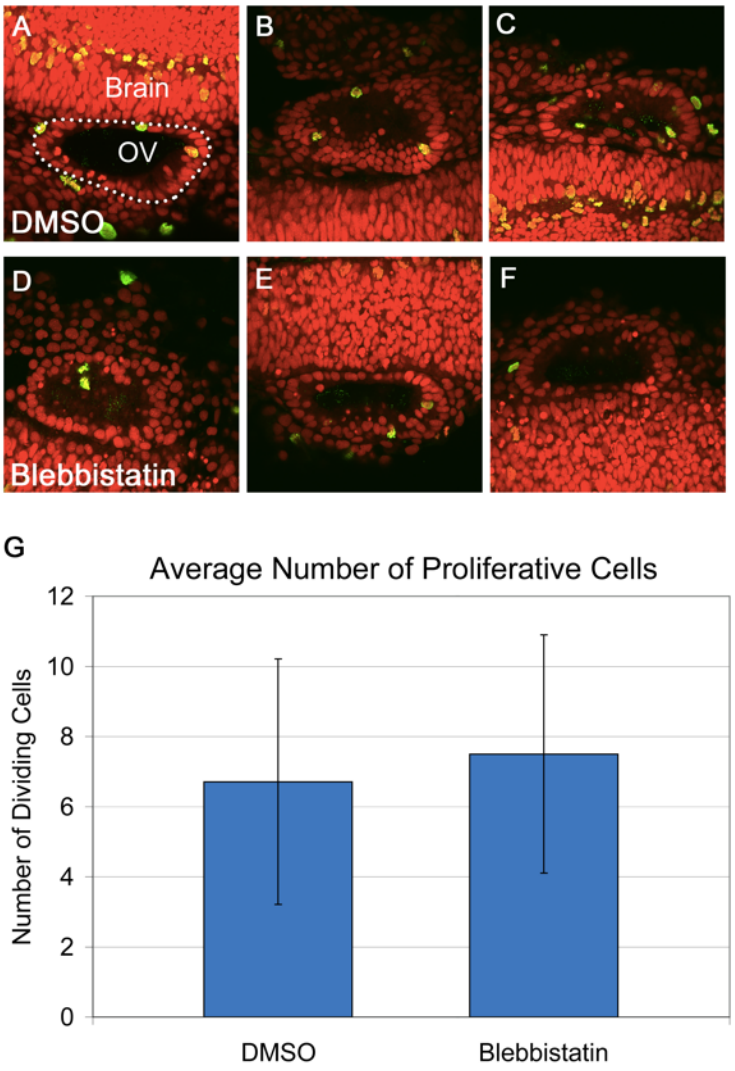

Fig. 9: Myosin II is not required for normal cell proliferation in the developing ear. (A - F) 16 hpf embryos were treated with 50 mM blebbistatin or DMSO control for three hours. Embryos were then washed, fixed at 24 hpf, and immunostained for phosphorylated histone H3 to label nuclei of proliferative cells (green) and counterstained with propidium iodide to label all nuclei (red). Anterior is to the left in all images. (A - C) Representative confocal images of DMSO-treated embryos. (A) The dotted line surrounds the outside border of the otic vesicle (OV) epithelium. (D - F) Representative confocal images of blebbistatin-treated embryos. (G) Graph of the average number of proliferative cells in the ear of embryos treated with DMSO or blebbistatin. DMSO: n=12; blebbistatin: n=7. Error bars indicate standard deviation. Statistical analysis showed no significant difference between DMSO and blebbistatin treatments.

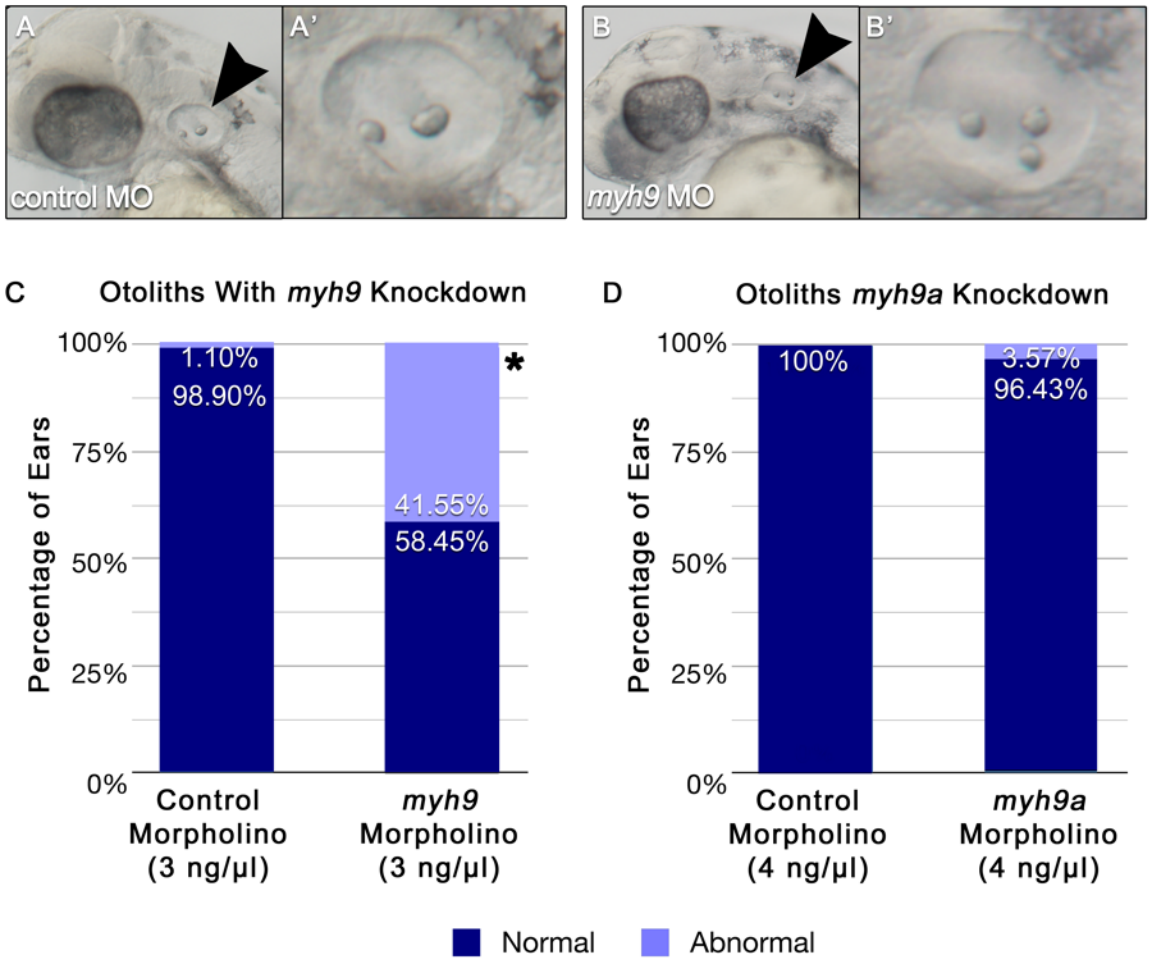

Fig. 10: NMIIA is required for normal otolith formation in the developing ear. Embryos were injected with control, *myh9*, or *myh9a* morpholino at the one- to two-cell stage, then raised to 36 hpf. (A - B) Black arrowheads indicate the developing ear. (A) 36 hpf control embryo displaying normal otolith number. (A') Magnification of the ear from image A. (B) 36 hpf *myh9* morphant embryo displaying an abnormal third otolith. (B') Magnification of the ear from image B. White arrowhead shows the third otolith. (C) Graph of the percentages of normal and abnormal numbers of otoliths per ear at 36 hpf when embryos were injected with control or *myh9* morpholino. Control morpholino: n=272; *myh9* morpholino: n=219. Asterisks indicate significance as tested using Fisher's exact test of independence for 2 x 2 tables at a significance level of 0.0001. (D) Graph of the percentage of normal and abnormal numbers of otoliths per ear at 36 hpf when embryos were injected with control or *myh9a* morpholino at the one to two cell stage. Control morpholino: n=146; *myh9a* morpholino: n=224. Significance testing showed no significant difference between control-injected and *myh9a*-injected embryos.

Chapter 3: Analysis of the Roles of Non-Muscle Myosin IIA in the Development and Function of Cilia in the Ear

Introduction

The mechanisms for how *MYH9* mutations lead to deafness in humans as a symptom of *MYH9*-related diseases is unknown. We have demonstrated that knockdown of the *myh9* gene, which encodes for non-muscle myosin IIA (NMIIA), in zebrafish results in the phenotype of an abnormal otolith number in approximately 40% of ears analyzed compared to control ears (Chapter 2). It has also been shown that otolith development is critically dependent on fluid currents in the otic vesicle generated by the force of beating cilia (Wu et al., 2011), and that loss of function of genes involved in ciliary motility results in mutant phenotypes affecting otolith number, size, and position (Colantonio et al., 2009; Stooke-Vaughan et al., 2012; Wu et al., 2011; Yu et al., 2011). Therefore, we hypothesized that the mechanism underlying the *myh9* loss-of-function abnormal otolith phenotype is a defect in the development or function of otic vesicle cilia, and we are testing this hypothesis using the zebrafish as a model system.

Cilia are composed of a microtubule core known as the axoneme, which is covered with plasma membrane continuous with that of the cell body (Fig. 6). The axoneme is anchored to the apical cell membrane by basal bodies, which are a pair of specialized centrioles (Ainsworth, 2007). In polarized epithelia, the correct orientation of the cilia and their basal bodies is determined by translational and rotational polarity. As described by Mirzadeh et al. (2010), translational polarity refers to the position of basal bodies near the apical surface of the cell, and rotational polarity describes the angle of individual basal bodies with respect to

their long axis (Fig. 6). Either of these two polarities can affect the tilt of the long axis of a cilium (Mirzadeh et al., 2010). Here we also use the term perpendicular rotation as described by Mirkovic et al. (2012) to refer to the rotational movement of cells within the apical surface of a tissue. While it is known that correct orientation of cilia and their basal bodies is necessary to achieve normal fluid flow (Marshall & Kintner, 2008), the cellular mechanisms responsible are not completely understood.

Several experiments have linked NMII to ciliary polarity. Hirota et al. (2010) found that NMII is required for an anterior translational polarity of ciliary basal bodies in mouse ependymal cells, and that this polarity results in a posterior tilt in the associated cilium. NMII has also been implicated in the movement of centrosomes into the leading process of migrating neurons (Solecki et al., 2009). Finally, it has been shown during establishment of basal body orientation in the quail oviduct that non-muscle myosin localizes to basal feet, which are projections of the ciliary basal bodies that anchor the axoneme into the apical cytoskeleton and point in the direction of ciliary beating (Fig. 6) (Lemullois et al., 1987; Mirkovic et al., 2012).

To test whether NMIIA contributes to the development and function of the cilia of the otic vesicle, as a potential mechanism causing the *myh9* loss-of-function phenotype, we performed experiments to assess the role of *myh9* in ciliogenesis, ciliary motility, and ciliary polarity.

Materials and Methods

Animals

All experiments were conducted using wild-type AB zebrafish. Embryonic stages are given as hours post fertilization (hpf) or days post post fertilization (dpf). Standard procedures were used for zebrafish maintenance, husbandry and staging (Kimmel et al., 1995).

Morpholino (MO) injections

Splice-site blocking morpholinos (Gene Tools) were dissolved in water and injected into one- to two-cell stage embryos in combination with membrane targeting GFP (mGFP). Morpholinos and their sequences, targeted splice sites, and concentrations used are as follows:

• *myh9* MO: 5'- ATGTCTGAAACAGTCGTTTACAAGC-3'; targets the zebrafish *myh9* gene at EXON6-intron6 boundary. It was used at 3 ng/µl for all experiments. The *myh9* sequence information is based on zebrafish Ensembl transcript ENSDART00000137105.

• *myh9a* MO: 5'-AGCAAGAGAGACTTACAAATCGAGA-3'; targets the zebrafish *myh9a* gene at intron1-EXON2 boundary. It was used at 4 ng/µl for all experiments. The *myh9a* sequence information is based on zebrafish Ensembl transcript ENSDART00000149823.

• standard control MO: 5′-CCTCTTACCTCAGTTACAATTTATA-3′; has no target. It was used at a concentration matching that of any experimental MO (*myh9* MO or *myh9a* MO).

• *p53* MO: GCGCCATTGCTTTTGCAAGAATTG-3'; targets the zebrafish *p53* gene. It was only used in conjunction with *myh9* knock down experiments (*myh9* MO and control MO) at an equal concentration to the test morpholino (Robu et al., 2007).

Immunohistochemistry

Embryos were fixed in Dents solution (80% methanol, 20% DMSO, used with anti-NMIIA) or in 4% paraformaldehyde (used with anti-acetylated tubulin and anti-gamma tubulin) for two hours at room temperature or overnight at 4ºC, blocked in 10% goat serum and 0.1% BSA in PBT overnight, incubated overnight in primary antibody (anti-NMIIA, M8064, Sigma-Aldrich, 1:500; or anti-acetylated tubulin, T6793, Sigma-Aldrich, 1:1000; or anti-gamma tubulin, T6557, Sigma-Aldrich, 1:1000), then incubated overnight in secondary antibody (goat anti-rabbit IgG conjugated with Alexa Fluor 488, Invitrogen, A11008, 1:500, used with anti-NMIIA; or goat anti-mouse IgG conjugated with Alexa Fluor 555, Invitrogen, A21422, 1:500, used with anti-acetylated tubulin and anti-gamma tubulin), some in combination with Alexa Fluor 488 phalloidin (Invitrogen, A12379, 1:1000). Embryos were mounted in glycerol and imaged using a Nikon CS2 laser-scanning confocal microscope. Images were analyzed with Nikon Elements software and Photoshop (Adobe).

Colocalization analysis

Whole confocal stacks of the zebrafish otic vesicle were cropped in three dimensions into sub-stacks of planar apical membrane of the otic vesicle epithelium. All included cells were exposed to the lumen of the otic vesicle. Sub-stacks ranged in depth for these cells from the apical membrane through the basal body. Sub-stacks were imported into ImageJ, and the “objects based methods” setting of the JACoP 2.0 plugin was used to determine Pearson’s coefficient, the overlap coefficient, and the total colocalization between 3D objects between two channels.

Three-dimensional (3D) tissue reconstruction for assessment of translational polarity of ciliary basal bodies

Confocal images of the otic vesicle were imported into ImageJ, and the “3D Viewer” plugin was used to create and export surface models to Maya (Autodesk) for 3D analysis of translational polarity. A line was drawn in 3D space in Maya between the two pairs of hair cells to establish a consistent direction for measurement of distances. This line was duplicated and translated in 3D space to intersect the center of the basal body of a cell to be analyzed and projected onto the apical surface of the cell. Two measurements were made along the line: the distance across the cell, and the distance from the basal body to the apical membrane edge. The value of the distance of the basal body to the apical membrane edge was divided by the distance across the entire cell to yield a percentage of distance of the basal body along the line. The line was then

rotated 90º about the basal body and this procedure was repeated to generate a second position of the basal body in another direction. The standard deviation was taken of five cells analyzed in this way from the same region of the otic vesicle to determine the consistency of the location of the basal bodies in that region. Standard deviations from control and *myh9* morphant groups were averaged and compared.

Scanning electron microscopy (SEM)

4 dpf zebrafish larvae were fixed in modified Karnovsky's fixative (2% paraformaldehyde and 2.5% glutaraldehyde in 0.1M cacodylate buffer, pH 7.4) for four days at room temperature, rinsed in cacodylate buffer, then post-fixed in 1% osmium tetroxide dissolved in PBS for 2 hours at room temperature. The larvae were dehydrated in a graded series of ethanol, during which time they were placed in an ultrasonic bath for 2 minutes to remove neuromast cupulas, and then critical point dried in carbon dioxide (Leica Microsystems, Balzers CPD 020). Embryos were each mounted on a 15 mm aluminum stub using double-sided tape, sputter coated with 4 nm of iridium (Emitech, K575X sputter coater), and imaged with a scanning electron microscope at 1.0 - 3.0 kV (Hitachi, S-4800 FE-SEM).

Imaging

All live confocal imaging was conducted as previously described (Graeden & Sive, 2009) using a Nikon CS2 scanning confocal and Nikon Elements software.

Live differential interference contrast (DIC) imaging was conducted on an AxioObserver Z1 microscope (Zeiss) and recorded by ORCA-Flash 4.0 camera (Hamamatsu) at ~300 frames per second using Zen 2012 software (Zeiss). All images were processed using Nikon Elements software or Photoshop (Adobe); all videos were processed using After Effects (Adobe).

Motility Analysis

Embryos were mounted laterally on a glass slide in a drop of tricaine mesylate (Sigma-Aldrich, E10521, 4%) between two 22 mm square coverslips, and a 25 x 60 mm coverslip was placed on top of the square coverslips to bridge the space and contact the embryo. Analysis of ciliary movement was performed on DIC microscopy videos in After Effects (Adobe) by using the brush tool to mark the position of the tip of a motile cilium at its greatest distances from the base of the cilium across five cycles of movement. These marks were merged into the last frame of the video, and the frame was exported as an image to Photoshop (Adobe) and the distance between the furthest pair of marks was measured using the measure tool. Time was recorded by subtracting the time in seconds of the video timecode at the first frame of analysis from the time of the last frame of analysis. Speed was determined by dividing the average distance transversed in one cycle of ciliary movement by the average time for one cycle of ciliary movement.

Statistical Analysis

Significance testing of differences between control and morphant embryos in cilia number, cilia length, translational polarity, distance of ciliary movement, time for one ciliary beat cycle and ciliary beat frequency was conducted using the Mann-Whitney *U* test at a significance level of 0.05. Colocalization of NMIIA protein and ciliary basal bodies was analyzed using Pearson's coefficient and the overlap coefficient as described below (Bolte and Cordelieres, 2006):

Given that channel A and channel B grey values of voxel i will be noted Ai & Bi respectively and the corresponding average intensities over the full image noted a & b,

Pearson's coefficient = (Si ((Ai-a)x(Bi-b)))/…(Si (Ai-a)²x Si (Bi-b)²)

Overlap coefficient = (Si (AixBi))/…(Si (Ai-a)²x Si (Bi-b)²)

Results

NMIIA colocalizes with ciliary basal bodies.

We initiated these studies by asking where NMIIA was localized in the developing otic vesicle. Based on the role for NMII in basal body translational polarity in ependymal cells, we hypothesized that NMIIA would be found in close proximity to ciliary basal bodies.

Wild type embryos were fixed at 24 hpf and then immunostained with NMIIA antibody and gamma tubulin antibody to visualize ciliary basal bodies. Whole confocal stacks of the zebrafish otic vesicle were cropped in three dimensions into sub-stacks to visualize planar apical membrane of the otic

vesicle epithelium (Fig. 11A - C'). NMIIA exhibited a punctate localization near the apical membrane which appeared to overlap the signal of basal bodies in many of the epithelial cells. Co-localization analysis of NMIIA with basal bodies was then performed using the JACoP 2.0 plugin for ImageJ to determine Pearson's coefficient, the overlap coefficient, and the total colocalization between 3D objects between two channels (Fig. 11D).

Pearson's coefficient indicates the correlation of intensity distribution between confocal channels; values range from -1 to 1; values indicating colocalization range from 0.5 to 1 (Zinchuk & Zinchuk, 2008). Our analysis of Pearson's coefficient resulted in a value of 0.64, which indicated moderate colocalization of NMIIA and gamma tubulin staining. The overlap coefficient indicates the actual overlap of signals; values range from 0 to 1, and values indicating colocalization range from 0.6 to 1.0 (Zinchuk & Zinchuk, 2008). The overlap coefficient in our analysis yielded a value of 0.9, which demonstrated a moderate to high degree of colocalization. The last analysis of localization separated the signal in both confocal channels into the categories of "background" and "objects", where background is defined as the 3D volume lacking significant signal and which contains objects, and objects are defined as self-contained regions of adjacent voxels with significant signal. Locations of objects were compared between the centers of their volumes, and these centers were considered to be colocalized if within a reference 3D distance calculated as previously described (Bolte & Cordelieres, 2006). Results of the analysis to determine the percentage of NMIIA objects colocalizing with basal body objects

was approximately 31%. Based on the results of these three analyses, we conclude that NMIIA and basal bodies colocalize in approximately one-third of the epithelial cells of the zebrafish otic vesicle at 24 hpf.

NMIIA is not required for ciliogenesis.

To test our hypothesis that defects exists in the development and function of cilia in the developing zebrafish ear with *myh9* loss-of-function, we began by asking if NMIIA plays a role in otic vesicle ciliogenesis. We hypothesized that NMIIA may be required for ciliogenesis by having a role in clearing actin from the site of new cilia formation, organizing a peripheral actin scaffold to help secure basal bodies and the axoneme, or by assisting in extension of the cell membrane to serve as ciliary membrane. Therefore, we examined cilia formation and number in the otic vesicle in *myh9* loss-of-function embryos.

Embryos were injected with control or *myh9* morpholino at the one- to two-cell stage and fixed at 24 hpf. Embryos were then immunostained for acetylated tubulin to label cilia and stained with fluorescent phalloidin to label actin. Whole otic vesicles were imaged using confocal microscopy (Figs. 12A - B'). We first analyzed the number of cilia by counting all cilia of the otic vesicle and averages were compared between control and morphant embryos (Fig. 12C). Next, we analyzed cilia length by taking 3D measurements of two cilia populations within the vesicle. We measured the tether cilia found on the developing hair cells and we measured cilia on cells surrounding the tether cilium hair cells, within two cell distances away. We found that both control and morphant embryos had

approximately 225 cilia per ear (Fig. 12C). We found that tether cilia were approximately 7 μm in length (Fig. 12D), and cilia on the cells neighboring the tether cilia hair cells were approximately 4 μm in length (Fig. 12D). We did not find any differences between control and *myh9* morphant cilia lengths in either population. These results indicate that NMIIA is not required for cilia formation, normal cilia number, nor for normal cilia length in the zebrafish otic vesicle.

NMIIA is not required for normal ciliary beat amplitude nor frequency.

After demonstrating that NMIIA is not required for ciliogenesis, we next wanted to determine if *myh9* had a role in the movement of cilia. The movement of cilia in the otic vesicle has been shown to be responsible for propagating currents that move otolith precursor particles toward the anterior and posterior poles of the otic vesicle (Wu et al., 2011). At the poles the precursor particles attach to the tether kinocilia of the hair cells and agglomerate, giving rise to two otoliths (Riley & Phillips, 2003).

In order to test ciliary motility in our *myh9* loss-of-function embryos, we recorded high-speed videos (~300 frames/sec) of cilia in the zebrafish otic vesicle at 24 hpf using differential interference contrast (DIC) microscopic imaging (Figs. 13A - D). By using this time point, we were able to exclude short motile cilia from our analysis, since they disappear from the otic vesicle at 24 hpf (Riley et al., 1997). These videos were used to analyze motile cilia detected at any position within the otic vesicle epithelium; in some instances more than one cilium was analyzed per ear and treated as a separate data point. We compared

control and morphant embryo ciliary motility by quantifying the average distance of movement of cilia tips, the average time for one 360 degree rotation of a cilium, and the average ciliary beat speed. Results indicated that both control and *myh9* morphant embryos had an approximate average distance of ciliary movement of 4 μm (Fig. 13E), an average ciliary beat cycle timing of 0.03 s (Fig. 13F), and an average speed of 140 μm/s (Fig. 13G). While our measurement of distance is within the published range (Wu et al., 2011), our finding of ciliary speed is approximately 4 times greater than published reports. Based on these experiments, our results suggest that NMIIA is not required to establish normal ciliary beat amplitude, time, or speed in the otic vesicle.

NMIIA is not required for translational polarity of ciliary basal bodies.

The polarity of the ciliary basal body pair determines the direction in which a motile cilium beats (Mirkovic et al., 2012; Nonaka et al., 2005). This in turn affects the direction of fluid movement caused by the motile cilium (Nonaka et al., 2005). In the mammalian embryonic patterning organ called the node, it has been found that basal bodies of motile cilia are initially positioned centrally but later move to the posterior side of the cell, resulting in a posterior tilt which has been shown to be required for normal leftward fluid flow (Hashimoto et al., 2010). Since we found that NMIIA is localized at the basal body, but the motility of the cilia appears normal, we hypothesized that NMIIA may play a similar role in ciliary translational polarity in the otic vesicle.

To test this hypothesis, control and *myh9* morpholino injected embryos were fixed at 24 hpf and immunostained for gamma tubulin to label ciliary basal bodies and stained with fluorescent phalloidin to label actin (Figs. 14A - B'). Embryos were imaged using confocal microscopy, and resultant z-stacks were reconstructed in three dimensions for analysis. To analyze translational polarity, we determined the position of ciliary basal bodies within the apical membrane of the otic vesicle epithelium. In order to determine position, a line was drawn between the two pairs of hair cells in 3D space to establish one consistent direction for measurement of distances (Fig. 14C). This line was duplicated and translated in 3D space to intersect the center of the basal body of each cell to be analyzed and was projected onto the apical surface of the cell (Fig. 14C', blue lines). Two measurements were made along the line: the distance across the cell (apical cell surface diameter), and the distance from the basal body to the edge of the apical membrane. The value of the distance of the basal body to the apical membrane edge was divided by the apical cell surface diameter to yield a percentage of distance of the basal body along the line (Fig. 14C'', blue line). The line was then rotated 90º about the basal body and this procedure was repeated to generate a second position of the basal body in a second direction (Figs. 14C' - C'', purple lines). Measuring along two sets of parallel lines drawn through the basal bodies of different cells in the same region allowed for a directionally consistent measurement of distance of the basal body from the apical membrane edge in two directions perpendicular to one another.

The standard deviation was determined for five cells analyzed in this way, from the region surrounding the same hair cell pair of the otic vesicle, to determine the consistency of the location of the basal bodies in that region. Standard deviations from control and *myh9* morphant groups were averaged and compared. Our results indicated that both control and morphant embryos showed variability in the apical position of their ciliary basal bodies of approximately 0.15 (Fig. 14D). Graphing of data with a box plot revealed no additional details of the data distribution. As a result of this finding, we concluded NMIIA is not required for translational polarity of ciliary basal bodies as tested by this method.

NMIIA is not required for perpendicular rotation in hair cells.

Having found that NMIIA is not involved in translational polarity of ciliary basal bodies, we aimed to increase our understanding of the role of NMIIA in establishing PCP more generally. To accomplish this, we tested the role of NMIIA in establishing the perpendicular rotation of hair cells in the zebrafish inner ear and lateral line. While these experiments do not address our main focus of polarity in ciliary basal bodies, they do test alternate roles of NMIIA in establishing polarity of ciliated cells in the inner ear. We hypothesized that if NMIIA is necessary for perpendicular rotation of hair cells, it is possible that it also has a role in the perpendicular rotation of otic vesicle epithelial cells, and could therefore affect the beat direction of cells bearing a tilted motile cilium.

We performed three sets of experiments to test the role of NMIIA in the perpendicular rotation of hair cells. We used confocal microscopy to analyze hair

cells of the otic vesicle at 24 hpf, confocal microscopy to analyze hair cells of the lateral line at 4 dpf, and scanning electron microscopy (SEM) to analyze hair cells of the lateral line at 4 dpf. The hair cells of the lateral line were used because they are morphologically and functionally similar to the hair cells of the inner ear, and are easy to access in imaging experiments (Mirkovic et al., 2012).

Control and *myh9* morphant embryos were fixed at 24 hpf and stained with fluorescent phalloidin to label actin. The rotational polarity of the otic vesicle hair cells was assessed by first drawing a line across the approximate center of the otic vesicle along the long axis of the lumen to be used as a reference for hair cell orientation (Fig. 15A). Next, a line was projected from the center of the stereociliary base through the center of the kinocilium base and the orientation angle of this line was observed from the blue reference line (Figs. 15B - C). We found in both control and *myh9* morphants that 83% of hair cell pairs had cells of a matching perpendicular rotation, but that this polarity did not match that of hair cell pairs in other otic vesicles.

Next, we analyzed the perpendicular rotation of hair cells in the lateral line. Each neuromast of the lateral line consists of two equally-sized populations of hair cells with perpendicular rotation oriented 180º relative to each other (Ghysen & Dambly-Chaudiere, 2007; Lopez-Schier et al., 2004). We hypothesized that this pattern of consistent perpendicular rotation would be disrupted in *myh9* hair cells, so that some of the hair cells would have perpendicular rotation out of a single axis of polarity. To test this hypothesis, hair cells of lateral line neuromasts were analyzed by confocal microscopy after fixing control and *myh9* morphant

embryos at 4 dpf and staining them with fluorescent phalloidin to label actin. Infraorbital neuromasts were then imaged (Figs. 15D - E'). We also analyzed hair cells of lateral line infraorbital neuromasts by SEM after fixing control and *myh9* morphant embryos at 4 dpf (Figs. 15F - I). In both experiments, the perpendicular rotation of hair cells was assessed by projecting a line from the center of the stereociliary base through the center of the kinocilium base. Orientation angles of these lines were compared between cells of a given neuromast to determine if any were polarized out of a single axis of perpendicular rotation. In both the confocal and SEM imaging experiments, controls and *myh9* morphants had normal perpendicular rotation, oriented 180º relative to each other (Figs. 15D - I').

Together these results led us to conclude that NMIIA is not required for perpendicular rotation in the hair cells of the zebrafish otic vesicle nor of the lateral line infraorbital neuromasts. Additional experiments will be necessary to demonstrate the role of NMIIA in the translational and rotational polarity of otic vesicle cilia.

Discussion

NMIIA colocalizes with ciliary basal bodies.

We demonstrate for the first time that NMIIA colocalizes with ciliary basal bodies in the otic vesicle epithelium. This finding led to the hypothesis that NMIIA may have a role in transporting basal bodies as a means to achieve normal translational and rotational polarity of cilia within the otic vesicle (Marshall & Kintner, 2008). Rotational and translational polarity determines the normal tilt

on a cilium to allow for linear propagation of fluid in the otic vesicle, as well as a normal beat direction. To discover whether NMIIA and basal bodies are directly associated or only located in close proximity, future work could include coimmunoprecipation experiments. Also, to discover whether NMIIA colocalizes with all ciliary basal bodies of the otic vesicle or only with those of motile cilia, immunostaining of a molecule for ciliary motility could be performed (see Future Directions, Chapter 4).

NMIIA is not required for ciliogenesis in the otic vesicle.

Our results showed no significant difference between control and *myh9* morphant embryos in the generation of normal cilia, suggesting that NMIIA is not required for ciliogenesis. The numbers and lengths of tether cilia and tether-neighboring cilia in control and loss-of-function embryos were consistent with previously published times, numbers, and lengths (Stooke-Vaughan et al., 2012; Yu et al., 2011). However, it is possible that ciliogenesis was disrupted in our experiments early in otic vesicle formation which was able to recover by the developmental time point we analyzed. If this is true, then our current results would have missed an earlier phenotype. It is also possible that NMIIA is only required for ciliogenesis of motile cilia. For the experiments presented here, we were not able to differentiate between motile and immotile cilia, potentially overlooking a subtle phenotype. Further investigation into the role for NMIIA in motile versus immotile cilia could provide additional clues for the role of NMIIA in ear development.

NMIIA is not required for normal ciliary beat amplitude nor speed.

The speed of beating cilia, and the distance of their stroke, are two parameters affecting hydrodynamics of the developing inner ear which account for otolith formation (Wu et al., 2011). For example, higher velocities in fluid currents nearer to the base of an otolith result in an asymmetric shape to a growing otolith (Wu et al., 2011), which may be necessary in later developmental stages for macular kinocilia to connect to the otolith (Karavitaki & Corey, 2010). Our data did not support a role for NMIIA in establishing normal ciliary beat amplitude nor frequency (Fig. 13). We found that the distance of travel of the cilium tip was approximately 4 μm in control and *myh9* morphant embryos, and this value is within the range published by Wu et al. (2011) of 3 - 5 μm.

The value we calculated for speed varied considerably from the findings of Wu and colleagues (2011). Our measure of speed was approximately 140 μm per second in control and *myh9* morphant embryos, compared with only 33 μm per second measured by Wu et al. There are at least three possible explanations for this discrepancy. First, Wu et al. used a different method to measure speed that employs the blinking optical trap technique. This technique relies on mathematical modeling, and is prone to errors from distortion caused by nearby walls in a fluid-filled vesicle (Svoboda & Block, 1994) and has difficulty accounting for the heterogeneity of biological data such as the texture of the surface of the epithelium, the spacing of cilia, and variations in ciliary beat pattern and direction (Smith et al., 2011). Wu and colleagues did not account for the true

ovoid morphology of the otic vesicle (Riley & Phillips, 2003); their measurements were approximated by an equation that admits analytical solutions inside a sphere, which is the shape they used to model the otic vesicle. Secondly, the data published did not indicate which population of motile cilia was analyzed: the short cilia that disappear at 24 hpf, or the polar cilia that are approximately 4 μm long and endure beyond 24 hpf, or both. Because our data were collected at 24 hpf, we excluded short motile cilia from our analysis. Lastly, Wu et al. analyzed embryos throughout the 18 - 24 hpf stages and considered all data to be equivalent, despite the dramatic changes occurring in the otic vesicle over these times, including the shortening of motile cilia, which could conceivably affect their speed. Also, as described above, Wu and colleagues did not account for the changing morphology of the otic vesicle epithelium over these times, and instead modeled the otic vesicle as a sphere.

An additional aspect of analysis differing in our experiments from those of Wu et al. concerns the location of motile cilia in the otic vesicle. Wu and colleagues found that the otolith is always located within a few microns of the motile cilia. However, we studied motile cilia located throughout the otic vesicle. For example, Fig. 13A shows a motile cilium belonging to control embryo located farther than 10 μm from an otolith. The hydrodynamic model of otic vesicle flow proposed by Wu et al. relies on the assumption that motile cilia are present only directly adjacent to otolith tether cilia to set up currents that attract particles and then stir them. This understanding of the location of motile cilia is based on the findings of Colantonio et al. (2009), which has been contradicted by other

research (Yu et al., 2011). A finding of motile cilia that are nonadjacent to tether hair cells may contradict the otic vesicle fluid-flow model of Wu and colleagues.

It is possible that our imaging techniques were not sensitive enough to detect more subtle changes or abnormalities in motile cilia movement; therefore, future studies are needed to examine ciliary movements at a higher frame rate.

NMIIA is not required for polarity of ciliary basal bodies or hair cells.

Translational polarity is known to be necessary to achieve tilt in motile cilia, which is in turn required for generating normal vesicle fluid flow (Mirzadeh et al., 2010; Wu et al., 2011). We hypothesized that NMIIA is required for translational polarity of otic vesicle basal bodies; however, our results did not demonstrate any significant difference in the translational polarity of ciliary basal bodies between control and morphant embryos as analyzed here (Fig. 14). Based on our results at the 24 hpf time point in cilia near the hair cell pairs, basal bodies are not translationally polarized, which suggests that translational polarity may not be responsible for tilt in these cilia. An alternate possibility is that these cilia instead achieve tilt through rotational polarization. An analysis of the role of NMIIA in rotational polarity of ciliary basal bodies, and the tilting of ciliary axonemes in the otic vesicle, are future directions that must yet be addressed.

To further study the role of NMIIA in PCP, we tested the perpendicular rotation of hair cells in the zebrafish otic vesicle and lateral line. Mirkovic et al. (2012) demonstrated that neuromast hair cells and their centrosomes (fated to later become ciliary basal bodies) can each undergo the form of rotational rearrangement we term perpendicular rotation. Only after these rotations are

complete do formation and asymmetric positioning of the hair cell kinocilia occur. We hypothesized that NMIIA is required for normal perpendicular rotation of hair cells in the zebrafish otic vesicle and lateral line neuromasts, and that perpendicular rotation might also be important in otic vesicle cells bearing motile cilia to control the direction of ciliary beating. Our results did not support this hypothesis: control and *myh9* morphant embryos showed no difference in perpendicular rotation in hair cells of both the otic vesicle and lateral line.

We also found that most control and *myh9* morphants had matching perpendicular rotation in the cells of a given hair cell pair, but that this polarity did not match that of hair cell pairs in other otic vesicles. This finding may seem aberrant, since it is known that a defined hair cell polarity within given sensory patches is critical to normal sensation (Faucherre et al., 2009). However, it has been demonstrated in the mouse vestibular system as well as the cochleas of mouse and chick that stereociliary bundles develop with an initial, non-random polarity that is biased towards the final orientation of each cell, and that later in development of these organs, individual stereociliary bundles gradually reorient to obtain their final orientation (Cotanche & Corwin 1991, Denman-Johnson & Forge 1999, Dabdoub et al., 2003). This is similar to what was found in zebrafish neuromast hair cells by Mirkovic et al. (2012). Our findings suggest that a similar process of reorientation may occur in hair cells of the zebrafish otic vesicle, although further testing is required to confirm this. It is known that zebrafish tether hair cells are precocious sensory hair cells that begin to function in sensation at 23 hpf (Tanimoto et al., 2011), and our analysis of polarity was

conducted at 24 hpf. It is possible that the small amount of time between attainment of sensory maturity of these hair cells and our analysis did not offer sufficient time for the cells to reorient for proper function.

Alternate methods of examination may offer additional understanding of the role of NMIIA in ciliary polarity. It is possible that the aspects of polarity we studied may be important only in alternate time points. For example, hair cells of the otic vesicle increase in number from two pairs at 24 hpf to 20 - 40 hair cells by 42 hpf (Haddon & Lewis, 1996); analysis of a large field of hair cells may lend additional insight into the perpendicular rotation of otic vesicle cells. It may also be that the 4 dpf time point at which we studied perpendicular rotation was too late to see a phenotype from *myh9* morpholino knockdown, or that embryos had recovered from an earlier aberrant phenotype by this time. Additionally, polarity may be important only in certain populations of otic vesicle cilia. For example, we were unable to distinguish ciliary basal bodies belonging to motile cilia from those of immotile cilia in our analysis of translational polarity.

Hypothesized role for NMIIA in cilia development and *MYH9*-related disease.

We previously concluded that NMIIA is required for proper ear development based on the phenotype we discovered of an abnormal otolith number in *myh9* loss-of-function embryos (Chapter 2). These findings led us to hypothesize that the role for *myh9* in otolith formation is through regulation of motile cilia of the otic vesicle. Here we have demonstrated that NMIIA colocalizes

with ciliary basal bodies in approximately one-third of otic vesicle epithelial cells, but that NMIIA is not responsible for ciliogenesis nor for ciliary motility in terms of speed or amplitude of ciliary beating (Fig. 11). These findings led us to hypothesize that NMIIA is necessary for establishing ciliary polarity. In motile cilia, translational or rotational polarity of the basal bodies is required to tilt cilia in order for the cilium to generate linear fluid flow within a vesicle (Mirzadeh et al., 2010; Wu et al., 2011), while perpendicular rotation may refine the direction of this linear fluid flow by turning the tilted cilium within the luminal surface of the vesicle. Here we have demonstrated that translational polarity is not dependent on NMIIA. Therefore, future experiments should be directed at discovering the role of NMIIA in establishing the rotational polarity of ciliary basal bodies.

Although we did not uncover a role for *myh9* in defining ciliary polarity in these studies, further experiments to investigate and identify a role for *myh9* in establishing ciliary polarity in zebrafish will serve as an important step toward understanding the causes of human *MYH9*-related disease. Polarity defects, as a result of *MYH9* mutations, may explain the disease symptoms that are found not only in the ear, but also in other ciliated organs affected by *MYH9*-related diseases including the kidney and the eye (Heath et al., 2001). During development of these organs, ciliary polarity may be necessary for the ability of motile cilia to distribute biological products akin to the distribution of otolith precursor particles in the developing ear, such as signaling molecules, as has been demonstrated in the brain (Sawamoto et al., 2006) and node (Okada et al., 2005). Additional work will be necessary to further characterize the role of *myh9*

in the polarity of cilia using the zebrafish as a model. This is discussed further in Chapter 4.

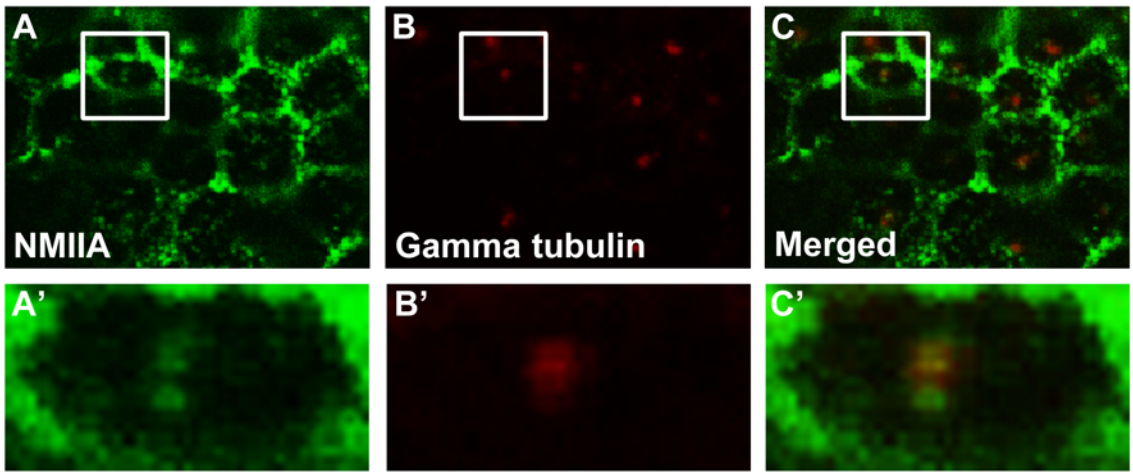

D

NMIIA and Ciliary Basal Body Colocalization Quantification Averages		
Pearson's Coefficient	Overlap Coefficient	Total Basal Body Objects Colocalizing with NMIIA Objects
0.64	0.90	30.51%

Fig. 11: NMIIA colocalizes with ciliary basal bodies. Embryos were immunostained with NMIIA antibody (green) and gamma tubulin antibody (red) to visualize ciliary basal bodies. (A - C) View of a region of the apical membrane of the developing otic vesicle at 24 hpf. Boxed regions identify the apical surface of one cell that has been magnified in A' - C'. (A, A') NMIIA staining. (B, B') Gamma tubulin staining. (C, C') Merged NMIIA and gamma tubulin staining signals showing colocalization. (D) NMIIA and ciliary basal body colocalization quantification analysis. Apical surface regions from the epithelium of otic vesicles from 11 embryos were analyzed using the "objects based methods" setting of the JACoP 2.0 plugin for ImageJ to determine Pearson's coefficient, the overlap coefficient, and the total colocalization between 3D objects in the two channels. Pearson's coefficient indicates the correlation of intensity distribution between confocal channels; values range from -1 to 1; values indicating colocalization range from 0.5 to 1. The overlap coefficient indicates the actual overlap of signals; values range from 0 to 1; values indicating colocalization range from 0.6 to 1.0. (Zinchuk V and Zinchuk O, 2008.) Average measures of Pearson's coefficient and the overlap coefficient indicate colocalization between the NMIIA and gamma tubulin signals.

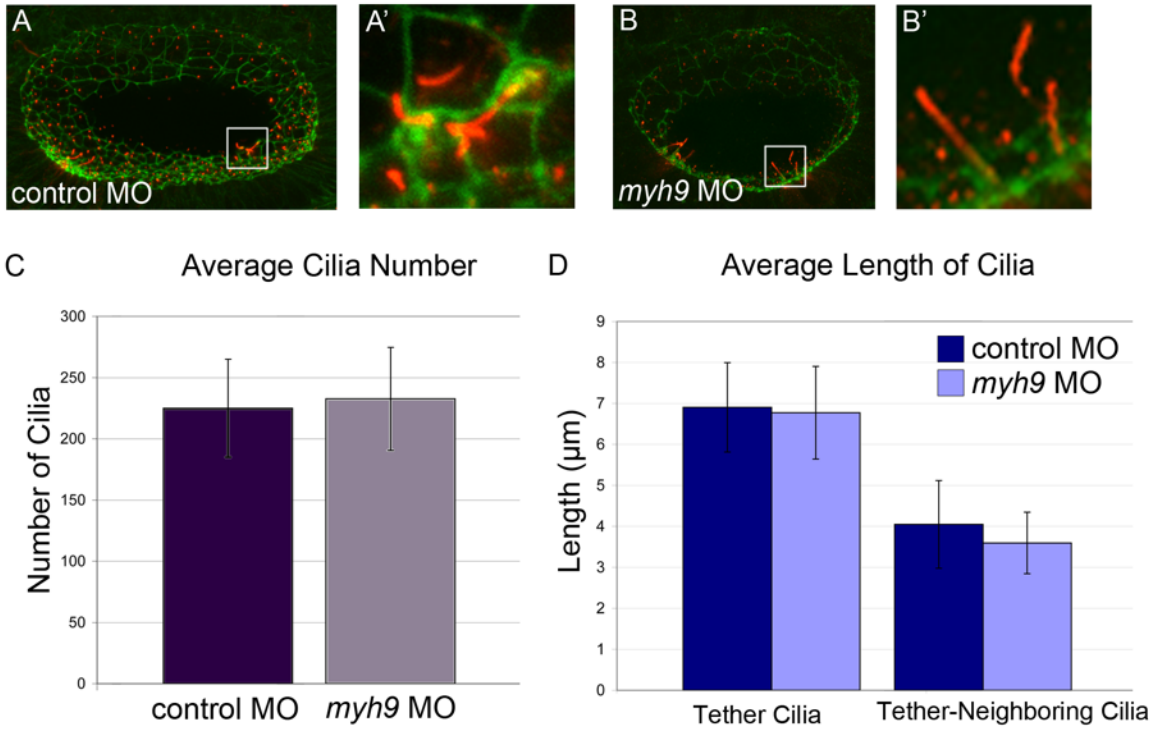

Fig. 12: NMIIA is not required for cilia formation nor proper cilia length. (A - B') Embryos were fixed at 24 hpf and immunostained for acetylated tubulin to label cilia (red) and stained with phalloidin to label actin (green). Images show a maximum intensity projection of slices of a confocal stack displaying measurable cilia. (A) Control morpholino-injected embryo. (A') Magnification of the boxed region in A. (B) *myh9* morphant embryo. (B') Magnification of the boxed region in B. (C) Graph of the average number of cilia throughout the otic vesicle at 24 hpf when embryos were injected with control or *myh9* morpholino. (D) Graph of the average length of tether cilia and cilia of cells within a distance of two cells from a tether cilium cell at 24 hpf when embryos were injected with control or *myh9* morpholino. (C - D) Error bars indicate standard deviation. Control: n=9; morphant: n=9. Significance testing showed no significant differences between control embryos and morphants.

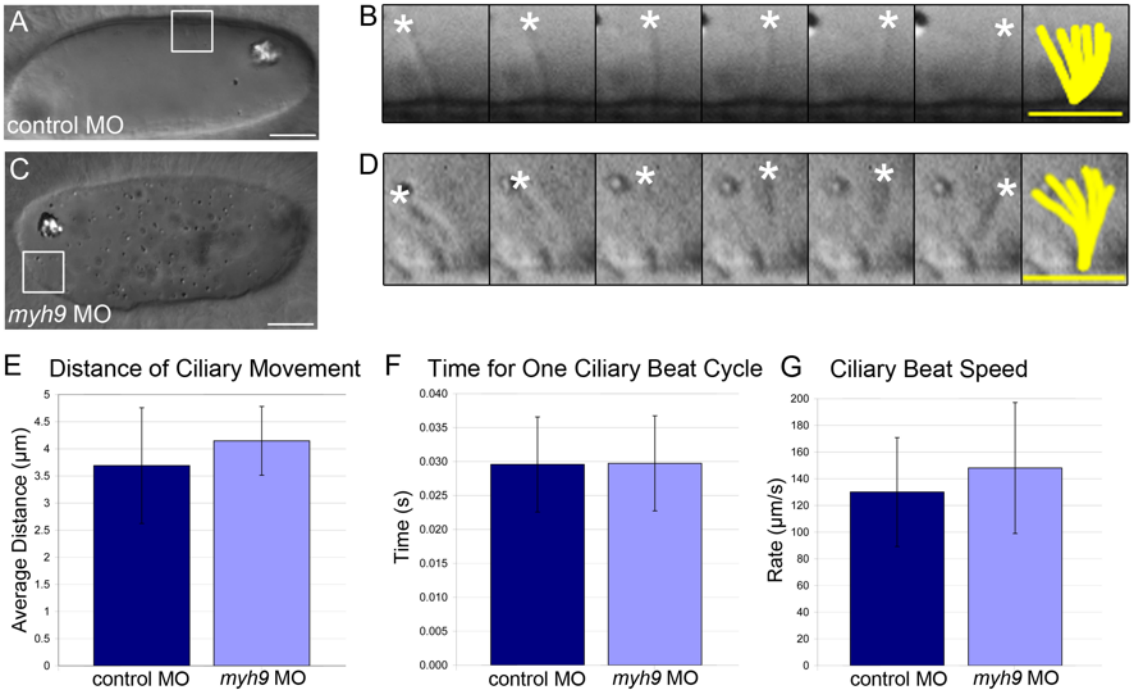

Fig. 13: NMIIA is not required for normal ciliary beat amplitude nor frequency. (A - D) DIC images of an otic vesicle from 24 hpf embryos injected with control (A-B) or *myh9* (C-D) morpholino. (B,D) Timelapse images showing magnification of the cilium from the boxed region in A and C, respectively. The tip of the cilium is indicated by asterisks in the first six frames. The last frame shows merged tracings in yellow of the cilium in the first six frames. (E) Graph comparing the average distance of ciliary movement between control and morphant embryos at 24 hpf. (F) Graph comparing the average time for one 360 degree rotation of a cilium between control and morphant embryos at 24 hpf. (G) Graph comparing the average ciliary beat speed between control and morphant embryos at 24 hpf. (E - G) Error bars indicate standard deviation. Significance testing showed no significant differences between control embryos and morphants. Control embryos: n = 7; cilia analyzed: n = 9. Morphant embryos: n=5; cilia analyzed: n = 7. (A,C) Scale bar = 10 µm. (B,D) Yellow scale bar = 5 µm.

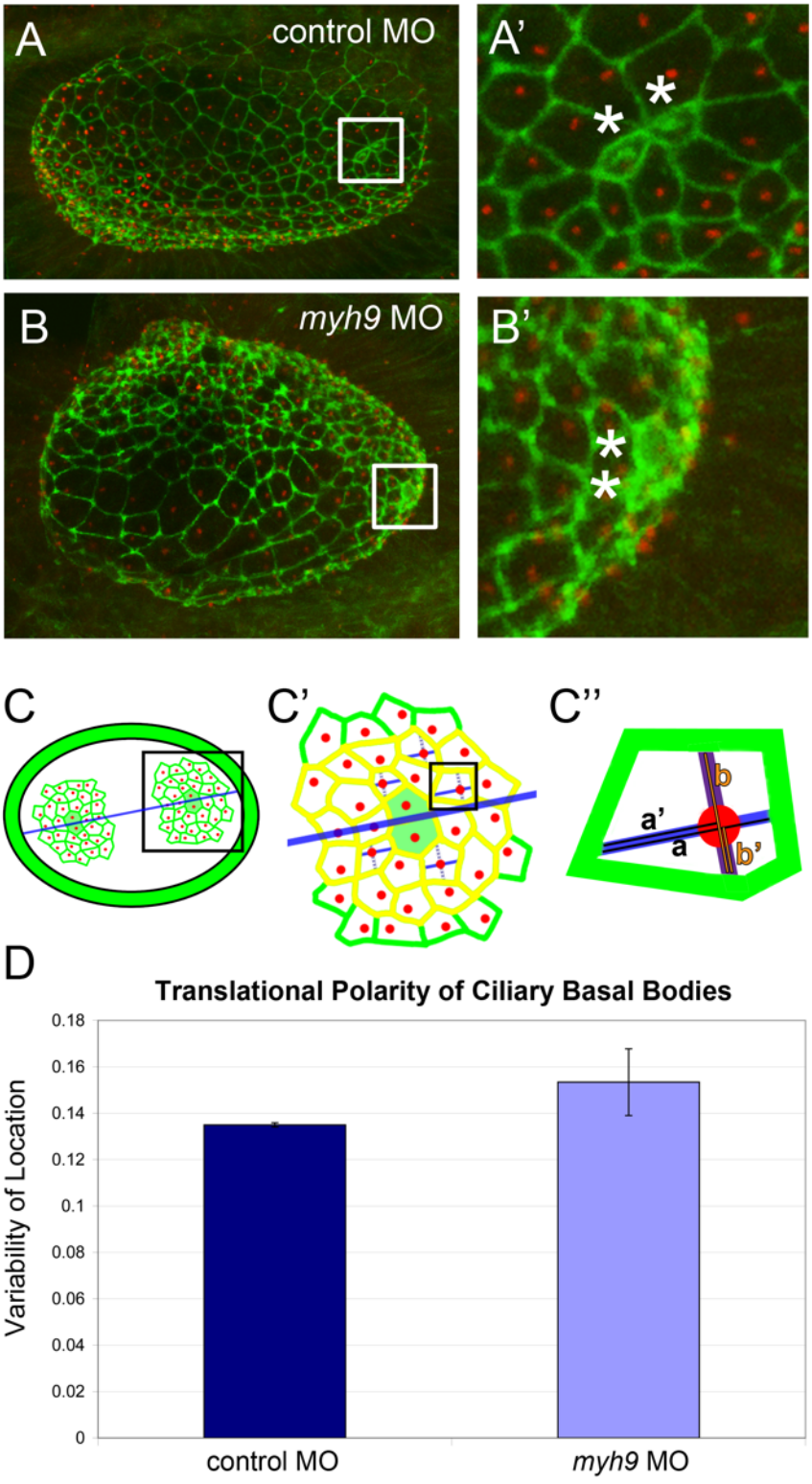

Fig. 14: NMIIA is not required for translational polarity of ciliary basal bodies. Control morpholino (A) and *myh9* morpholino (B) injected embryos were

fixed at 24 hpf and immunostained for gamma tubulin to label ciliary basal bodies (red) and stained with fluorescent phalloidin to label actin (green). (A', B') Magnification of the boxed region in A and B, respectively. Asterisks indicate hair cells. (C - C'') Diagram of the method for confocal data analysis. Z-stacks were reconstructed in three dimensions using the "3D Viewer" plugin in ImageJ to ensure accurate distance measurement. Green represents actin; red represents ciliary basal body pairs. (C) The otic vesicle with two regions of cells surrounding a hair cell pair (shaded cells) is shown. A line was drawn between the two pairs of hair cells (blue) to establish a consistent direction for measuring basal body location relative to the apical cell membrane. (C') Magnification of the boxed region in (C). Only those epithelial cells within two cell diameters of a hair cell pair were used for analysis, shown in yellow. Five cells were chosen for analysis in each hair cell region. (C'') Magnification of one cell from the boxed region in C'. Lines parallel to the reference line were drawn through the center of the basal body pair in each cell (thin blue lines) and lines perpendicular to the reference line were drawn through the basal body pair as well (dotted purple lines). Measuring along two sets of parallel lines drawn through the basal bodies of different cells allowed for a directionally consistent measurement of distance of the basal body from the lateral cell membrane in two directions (offset by 90º). Translational polarity values were calculated by dividing the distance a' by the distance a, and b' by b (shown in C''). The standard deviations of the distances from the cells of all analyzed regions were averaged and compared between control and morphant groups. (D) Graph of the translational polarity of ciliary basal bodies at 24 hpf when embryos were injected with control or *myh9* morpholino. Control embryos: n=8; morphant embryos: n=6. Error bars indicate standard error of the mean. Significance testing showed no significant differences between control embryos and morphants. Graphing of data with a box plot revealed no additional details of the data distribution.

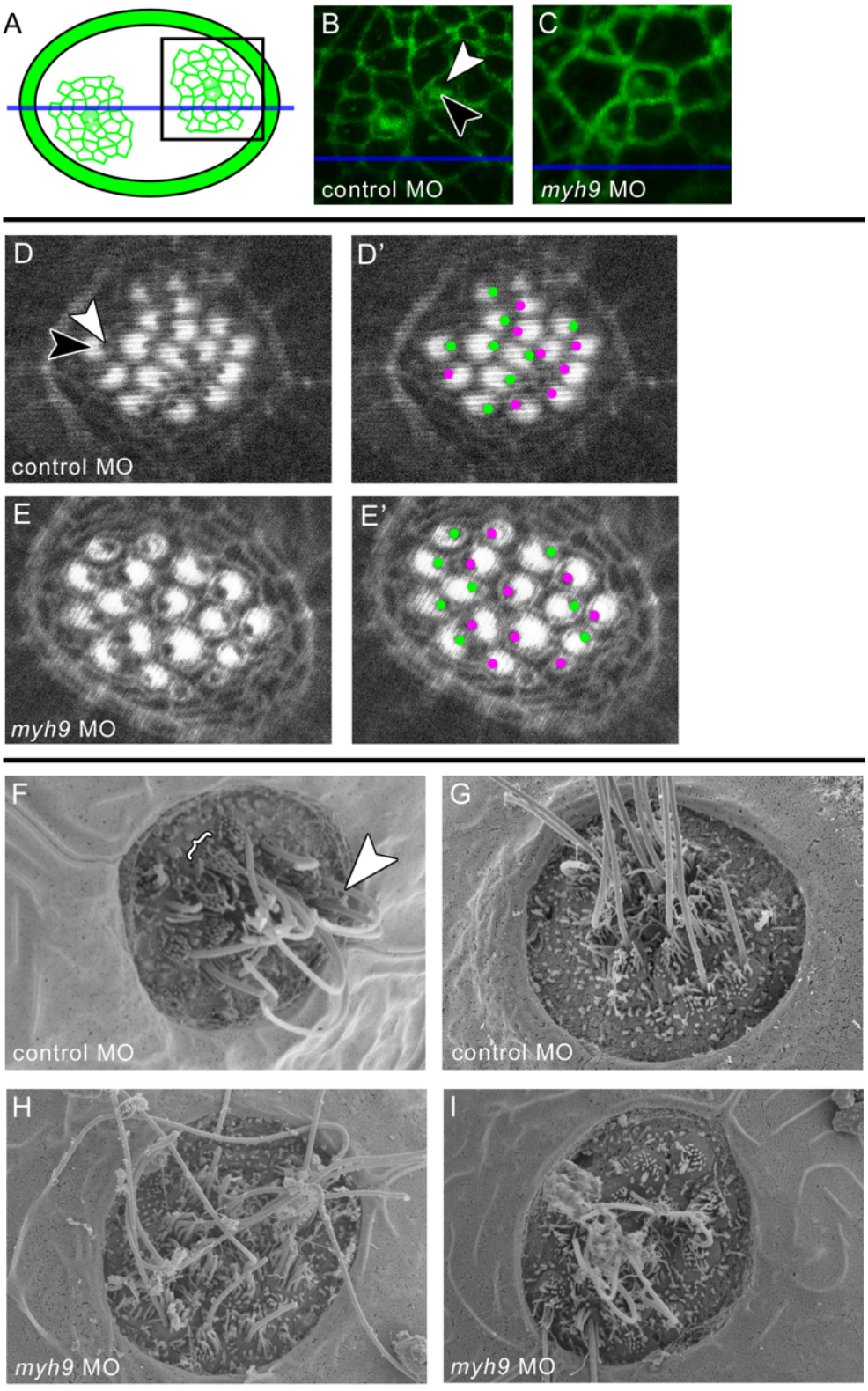

Fig. 15: NMIIA is not required for perpendicular rotation in hair cells. (A) Diagram of the otic vesicle at 24 hpf with two regions of cells surrounding a hair

cell pair (shaded cells). Green represents actin. A blue line is drawn across the approximate center of the otic vesicle along the long axis of the lumen to be used as a reference for hair cell orientation. (B - C) Embryos were fixed at 24 hpf and stained with fluorescent phalloidin to label actin (green). Micrographs display a region of the otic vesicle as indicated by the boxed region in A, and include a blue reference line as in A. The perpendicular rotation of hair cells was assessed by projecting a line from the center of the stereociliary base through the center of the kinocilium base. Orientation angles of these lines were observed from the blue reference line. (B) Control morpholino-injected embryo. Black arrowhead indicates the position of a hair cell stereociliary base; white arrowhead indicates the position of a hair cell kinocilium base. (C) *myh9* morphant embryo. (D - E') Embryos were fixed at 4 dpf and stained with fluorescent phalloidin to label actin. Infraorbital neuromasts were then imaged using confocal microscopy (>5 per embryo). The perpendicular rotation of hair cells was assessed by projecting a line from the center of the stereociliary base through the center of the kinocilium base. Orientation angles of these lines were compared between cells of a given neuromast. (D) Control morpholino-injected embryo. Black arrowhead indicates the position of a stereociliary base; white arrowhead indicates the position of a kinocilium base. (D') Green and magenta dots indicate the location of hair cell kinocilia of differing polarities in D. (E) *myh9* morphant embryo. (E') Green and magenta dots indicate the location of hair cell kinocilia of differing polarities in E. (F - I) Embryos were fixed at 4 dpf and infraorbital neuromasts were imaged using scanning electron microscopy. The perpendicular rotation of hair cells was assessed by projecting a line from the center of the stereociliary base through the center of the kinocilium base. Orientation angles of these lines were compared between cells of a given neuromast. (F - G) Control morpholino-injected embryos. (F) Arrowhead indicates a kinocilium; bracket indicates a stereociliary bundle. (H - I) *myh9* morphant embryos. (B - C) Control embryos: n=16; morphant embryos: n=15. (D - E) Control embryos: n=6; morphant embryos: n=6. (F - I) Control embryos: n=6; morphant embryos: n=4.

Chapter 4: General Conclusions and Future Directions

General Conclusions

The primary goal of this thesis was to examine the role of non-muscle myosin IIA (NMIIA) in zebrafish ear development and function as a means to study the molecular mechanisms of deafness associated with *MYH9*-related diseases. We found via loss-of-function experiments that NMIIA is required for formation of normal otolith numbers in the developing otic vesicle (Fig. 10). Based on abundant current studies, we hypothesized that this abnormal otolith phenotype with *myh9* loss-of-function was due to a defect in the motility of cilia in the developing zebrafish ear. To test this hypothesis, we first performed experiments to assess localization of NMIIA in the otic vesicle (Fig. 11). Next, we analyzed the role of NMIIA in ciliogenesis (Fig. 12) and the role for NMIIA in regulating motile cilia speed and distance of beating (Fig. 13). Results of these experiments demonstrated that NMIIA colocalizes with ciliary basal bodies, but is not required for ciliogenesis nor for normal cilia movement.

This finding led us to hypothesize that NMIIA is involved in establishing the polarity of ciliary basal bodies. It has been established that basal body translational polarity is necessary to establish ciliary tilt (Nonaka et al., 2005). Furthermore, ciliary tilt is necessary for linear fluid flow in a vesicle (Hashimoto et al., 2010), and proper fluid flow is necessary for normal otolith formation (Wu et al., 2011). Therefore, we hypothesized that our documented otolith phenotype was the result of defective basal body polarity in *myh9* loss-of-function embryos. Although the results of our experiments addressing polarity did not directly

support this hypothesis, we believe future experiments are necessary before a definitive conclusion can be drawn.

Future Directions

Additional experiments are required to determine the mechanism by which NMIIA regulates otolith formation in the developing ear. It has been established that otolith formation depends on cilia-induced fluid flow within the otic vesicle. Therefore, future experiments are set to address the hypothesis that *myh9* loss-of-function results in abnormal fluid flow within the otic vesicle. Additionally, abnormal fluid flow is hypothesized to be caused by abnormal movement of cilia, which in turn, could result from abnormal ciliary polarity that was not thoroughly investigated in this thesis (Fig. 16). Four areas of experimental methodology may be used to address this hypothesis. 1. High-speed differential interference contrast (DIC) imaging of cilia movement. 2. Tracking of otolith precursor particles within the otic vesicle using confocal microscopy. 3. Transmission electron microscopy (TEM) for analyzing basal body polarities combined with immunohistochemistry to detect proteins of interest to ciliary structure and function. 4. Scanning electron microscopy (SEM) to analyze ciliary tilt and hair cell organization in the otic vesicle. Each of these proposed experiments are discussed further below.

Experiments employing live DIC imaging would be used to compare several characteristics of motile cilia in the otic vesicle between control and *myh9* morphant embryos. All experiments would be done with consideration given to

the following categories: motile versus immotile cilia, motile polar cilia versus motile short cilia, cilia in an otolith-forming region versus those far from one, and the various developmental stages of embryos from 18 to 24 hpf. Of these, we believe distance from an otolith forming region to be the most important. Two parameters to be further studied with these distinctions in mind include the speed of cilia and the distance of travel during one ciliary beat cycle according to the methods already described in this thesis. An additional characteristic to explore is the direction of cilia movement, which could be accomplished by imaging ciliated cells at an angle perpendicular to their apical membrane in order to see the path traced by the tips of cilia. Also, the shape of the beat stroke could be analyzed by imaging beating cilia along their long axis. Finally, by changing the plane of focus and moving through the otic vesicle, it may be possible to count the total number of motile cilia. We note that it may be necessary to perform these experiments with equipment capable of higher resolution and frame capture rates to ensure that minute differences in motility are detected between control and morphant embryos.

Experiments tracking particles in the otic vesicle could be used to study the fluid flow generated by motile cilia to compare control and *myh9* morphant embryos. This could be accomplished through injection of fluorescent beads into the otic vesicle, or by labeling the otolith precursor particles by injecting FM1-43 dye (Tanimoto et al., 2011) and then imaging the vesicle using confocal microscopy. Confocal data could then be analyzed using manual tracking

methods, or through automatic tracking using computer software, in order to map the directions and speeds of the currents of the otic vesicle.

TEM analysis could be used for an assessment of ciliary polarity accurate to nanometer-scale resolution, as well as for immunohistochemical localization of proteins important for ciliary function. In terms of translational polarity, planar cell polarity measurements of distance from the edges of the apical membrane could be made in serial sections along directionally-consistent anteroposterior or ventrodorsal axes of the otic vesicle, as well as an apico-basal measurement of distance of the basal body from the apical membrane. Regarding rotational polarity, the angle of the basal body pairs relative to the apical surface could be measured. Lastly, transverse sections through cilia could demonstrate useful differences for distinguishing the types of cilia of the otic vesicle (for example, presence or absence of a central microtubule pair might differentiate immotile and motile cilia (Yu et al., 2011).

TEM combined with immunocytochemistry in sections cut through the epithelial cells of the otic vesicle on an apico-basal axis would be useful in identifying the localization of NMIIA and actin in or near cilia and ciliary basal bodies in order to study differences between control and *myh9* morphants. It could also be used to detect localization of ciliary motility proteins such as dynein, or the protein products of genes *gas8* or *dnaaf1*, both of which are components of the dynein regulatory complex and are required for ciliary motility (Colantonio et al., 2009; Stooke-Vaughan et al., 2012). A tangential benefit of immunocytochemistry using these dynein regulatory complex proteins is that if

they were found to localize to motile cilia but not immotile cilia, they could serve as markers in confocal immunostaining as well to differentiate classes of cilia.

A final mode of analysis employs SEM to detect differences in ciliary tilt and hair cell apical morphology between control and *myh9* morphant embryos by sectioning into the embryo to expose the otic vesicle lumen. First, SEM could be used to study the tilt of cilia throughout the otic vesicle, since ciliary axoneme tilt has been linked to normal otic vesicle fluid flow (Hashimoto et al., 2010). This can be accomplished by capturing electron micrographs of the same region of the otic vesicle epithelium at various angles by tilting the microscope stage, then combining all images using computer software to render a 3D reconstruction of the tissue for tilt angle measurement (Nonaka et al., 2005). One micrograph capturing the whole embryo can be used to measure the direction of the antero-posterior axis (Nonaka et al., 2005). Secondly, because *myh9* expression has been found in the stereocilia of mouse cochlear hair cells (Mhatre et al., 2006), SEM could be used to analyze hair cell integrity in terms of organization of stereocilia and kinocilia to address larger questions about the role of *myh9* in auditory sensation.

To increase the specificity and transferability of our *myh9* loss-of-function research in the zebrafish model to human *MYH9*-disease in future experiments, we intend to create a mutant line of zebrafish with mutations that mimic the human *MYH9* mutations that most frequently result in deafness. This could be accomplished through genomic engineering methods employing ZFN, CRISPR/Cas or TALEN nucleases (Gaj et al., 2013). Zebrafish mutants would also allow

us to screen for deafness in larval, juvenile, and adult fish, and if it is present, compare the deafness pathology of the mutant fish to that of the human. Genesis of *myh9* mutant zebrafish lines that replicate human *MYH9* mutations and the resulting hearing loss phenotype would serve as a useful tool for the experiments described above, as well as for screening potential drug therapies for *MYH9*-related disease.

Of the deafness-causing *MYH9* human mutations, we are especially interested in creating a zebrafish mutant with the amino acid substitution R705H, which causes autosomal dominant nonsyndromic deafness DFNA17 in humans (Kunishima & Saito, 2010). There are several reasons for this choice. First, approximately 70% of genetic deafness diseases are known to be nonsyndromic in nature (Nance, 2003). Secondly, this mutation is in the head domain of the NMIIA protein, a location that results in the most severe hearing phenotypes (Iwai et al., 2006). Also, unlike other deafness-causing *MYH9* mutations in humans, this mutation produces deafness invariably without complication by other disease symptoms. Finally, its effects have been traced to degeneration of the organ of Corti (Lalwani et al., 1997), which suggests that DNFA17 hearing loss may be the result of a defect in the formation and/or maintenance of organ of Corti hair cells (Mhatre et al., 2006).

The experimental results we have presented here are first steps toward determining the molecular mechanisms for how *MYH9* mutations cause disease in ciliated systems, specifically in the development of the inner ear. The activities of cilia, and the many varied biological processes they affect during development,

and in mature organisms, is a complex topic requiring additional research. Using the zebrafish otic vesicle as a model for ear development provides the tools necessary to analyze the development and function of the vertebrate ear and to address the symptom of deafness in *MYH9*-related diseases resulting from *MYH9* mutations. Although it is presently not known whether ciliary motility has a role in development of the mammalian otic vesicle, the work begun here may potentially be extended to the development and function of the human ear to enable understanding of the roles of non-muscle myosins in human deafness as a step toward its treatment. Overall these findings increase our understanding of the roles of NMIIA in the vertebrate ear and suggest that the regulation of ciliary motility should be further investigated.

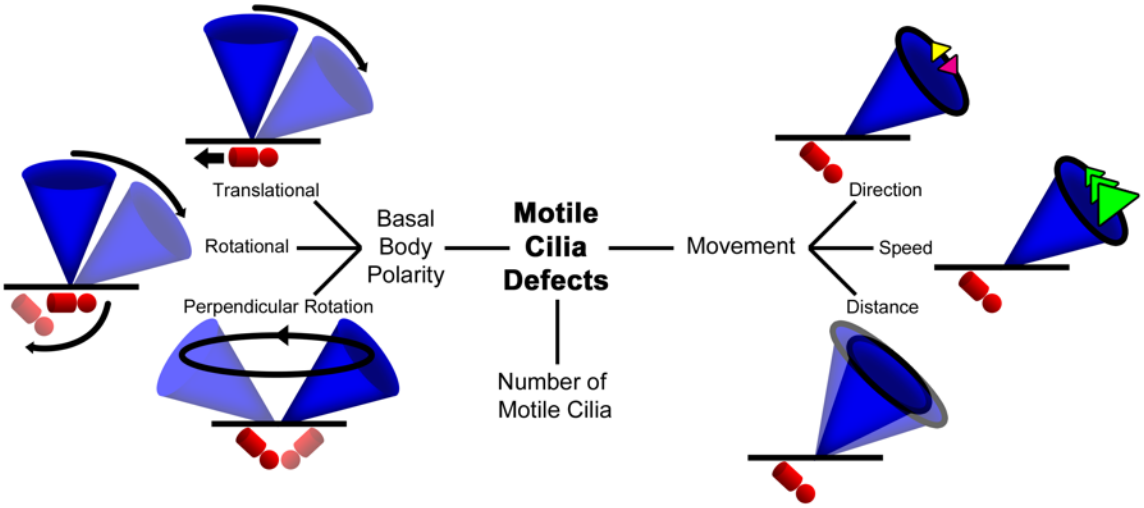

Fig. 16: Possible defects in motile cilia of the otic vesicle. Blue cones depict the 360º movement path of one motile cilium; red objects depict ciliary basal bodies. Motility defects may arise from an incorrect number of motile cilia, basal body polarity defects (translational or rotational), or defects in movement (direction, speed, or distance traveled). Yellow and magenta arrowheads indicate opposing directions of movement; nested green arrows indicate variance in speed. Results provide evidence that *myh9* is not responsible for translational or rotational polarity in the ear, nor for the movement of cilia in terms of speed or distance traveled in embryos aged between 22 - 24 hpf. Future experiments are needed to assess the role of *myh9* in determining the number of motile cilia, the direction of ciliary movement, and distinguishing the properties of motile cilia near an otolith from those of motile cilia distanced from an otolith. Repetition of existing motility experiments is also needed, using an imaging system capable of capturing data at a higher resolution and frame rate.

References

Aamar, E. and I. B. Dawid (2010). "Sox17 and chordin are required for formation of Kupffer's vesicle and left-right asymmetry determination in zebrafish." Dev Dyn **239**(11): 2980-2988.

Ainsworth, C. (2007). "Cilia: tails of the unexpected." Nature **448**(7154): 638-641.

Bang, P. I., W. F. Sewell and J. J. Malicki (2001). "Morphology and cell type heterogeneities of the inner ear epithelia in adult and juvenile zebrafish (Danio rerio)." J Comp Neurol **438**(2): 173-190.

Barua, B., A. Nagy, J. R. Sellers and S. E. Hitchcock-DeGregori (2014). "Regulation of Nonmuscle Myosin II by Tropomyosin." Biochemistry.

Bolte, S. and F. P. Cordelieres (2006). "A guided tour into subcellular colocalization analysis in light microscopy." J Microsc **224**(Pt 3): 213-232.

Brokaw, C. J. (2005). "Computer simulation of flagellar movement IX. Oscillation and symmetry breaking in a model for short flagella and nodal cilia." Cell Motil Cytoskeleton **60**(1): 35-47.

Busch-Nentwich, E., C. Sollner, H. Roehl and T. Nicolson (2004). "The deafness gene dfna5 is crucial for ugdh expression and HA production in the developing ear in zebrafish." Development **131**(4): 943-951.

Chang, W., J. V. Brigande, D. M. Fekete and D. K. Wu (2004). "The development of semicircular canals in the inner ear: role of FGFs in sensory cristae." Development **131**(17): 4201-4211.

Colantonio, J. R., J. Vermot, D. Wu, A. D. Langenbacher, S. Fraser, J. N. Chen and K. L. Hill (2009). "The dynein regulatory complex is required for ciliary motility and otolith biogenesis in the inner ear." Nature **457**(7226): 205-209.

Conti, M. A. and R. S. Adelstein (2008). "Nonmuscle myosin II moves in new directions." J Cell Sci **121**(Pt 1): 11-18.

Coombs, S., R. R. Fay and J. Janssen (1989). "Hot-film anemometry for measuring lateral line stimuli." J Acoust Soc Am **85**(5): 2185-2193.

Corwin, J. T. (1983). "Postembryonic growth of the macula neglecta auditory detector in the ray, Raja clavata: continual increases in hair cell number,

neural convergence, and physiological sensitivity." J Comp Neurol **217**(3): 345-356.

Cotanche, D. A. and J. T. Corwin (1991). "Stereociliary bundles reorient during hair cell development and regeneration in the chick cochlea." Hear Res **52**(2): 379-402.

Couly, G. F., P. M. Coltey and N. M. Le Douarin (1993). "The triple origin of skull in higher vertebrates: a study in quail-chick chimeras." Development **117**(2): 409-429.

Dabdoub, A., M. J. Donohue, A. Brennan, V. Wolf, M. Montcouquiol, D. A. Sassoon, J. C. Hseih, J. S. Rubin, P. C. Salinas and M. W. Kelley (2003). "Wnt signaling mediates reorientation of outer hair cell stereociliary bundles in the mammalian cochlea." Development **130**(11): 2375-2384.

Denman-Johnson, K. and A. Forge (1999). "Establishment of hair bundle polarity and orientation in the developing vestibular system of the mouse." J Neurocytol **28**(10-11): 821-835.

Eddinger, T. J. and D. P. Meer (2007). "Myosin II isoforms in smooth muscle: heterogeneity and function." Am J Physiol Cell Physiol **293**(2): C493-508.

Ernest, S., G. J. Rauch, P. Haffter, R. Geisler, C. Petit and T. Nicolson (2000). "Mariner is defective in myosin VIIA: a zebrafish model for human hereditary deafness." Hum Mol Genet **9**(14): 2189-2196.

Essner, J. J., J. D. Amack, M. K. Nyholm, E. B. Harris and H. J. Yost (2005). "Kupffer's vesicle is a ciliated organ of asymmetry in the zebrafish embryo that initiates left-right development of the brain, heart and gut." Development **132**(6): 1247-1260.

Faucherre, A., J. Pujol-Marti, K. Kawakami and H. Lopez-Schier (2009). "Afferent neurons of the zebrafish lateral line are strict selectors of hair-cell orientation." PLoS One **4**(2): e4477.

Fekete, D. M. and D. K. Wu (2002). "Revisiting cell fate specification in the inner ear." Curr Opin Neurobiol **12**(1): 35-42.

Fettiplace, R. and K. X. Kim (2014). "The Physiology of Mechanoelectrical Transduction Channels in Hearing." Physiol Rev **94**(3): 951-986.

Flicek, P., M. R. Amode, D. Barrell, K. Beal, K. Billis, S. Brent, D. Carvalho-Silva, P. Clapham, G. Coates, S. Fitzgerald, L. Gil, C. G. Giron, L. Gordon, T. Hourlier, S. Hunt, N. Johnson, T. Juettemann, A. K. Kahari, S. Keenan, E. Kulesha, F. J. Martin, T. Maurel, W. M. McLaren, D. N. Murphy, R. Nag, B.

Overduin, M. Pignatelli, B. Pritchard, E. Pritchard, H. S. Riat, M. Ruffier, D. Sheppard, K. Taylor, A. Thormann, S. J. Trevanion, A. Vullo, S. P. Wilder, M. Wilson, A. Zadissa, B. L. Aken, E. Birney, F. Cunningham, J. Harrow, J. Herrero, T. J. Hubbard, R. Kinsella, M. Muffato, A. Parker, G. Spudich, A. Yates, D. R. Zerbino and S. M. Searle (2014). "Ensembl 2014." Nucleic Acids Res **42**(Database issue): D749-755.

Fliegauf, M., T. Benzing and H. Omran (2007). "When cilia go bad: cilia defects and ciliopathies." Nat Rev Mol Cell Biol **8**(11): 880-893.

Fritzsch, B. and K. W. Beisel (2001). "Evolution and development of the vertebrate ear." Brain Res Bull **55**(6): 711-721.

Fritzsch, B., I. Silos-Santiago, L. M. Bianchi and I. Farinas (1997). "The role of neurotrophic factors in regulating the development of inner ear innervation." Trends Neurosci **20**(4): 159-164.

Gaj, T., C. A. Gersbach and C. F. Barbas, 3rd (2013). "ZFN, TALEN, and CRISPR/Cas-based methods for genome engineering." Trends Biotechnol **31**(7): 397-405.

Ghysen, A. and C. Dambly-Chaudiere (2007). "The lateral line microcosmos." Genes Dev **21**(17): 2118-2130.

Graeden, E. and H. Sive (2009). "Live imaging of the zebrafish embryonic brain by confocal microscopy." J Vis Exp(26).

Gregan, J., K. Lindner, L. Brimage, R. Franklin, M. Namdar, E. A. Hart, S. J. Aves and S. E. Kearsey (2003). "Fission yeast Cdc23/Mcm10 functions after pre-replicative complex formation to promote Cdc45 chromatin binding." Mol Biol Cell **14**(9): 3876-3887.

Groves, A. K. and M. Bronner-Fraser (2000). "Competence, specification and commitment in otic placode induction." Development **127**(16): 3489-3499.

Gutzman, J. H., S. Sahu and C. Kwas (2014). "Non-muscle myosin IIA and IIB differentially regulate cell shape changes in the zebrafish midbrain-hindbrain boundary during morphogenesis." [submitted].

Haddon, C. and J. Lewis (1996). "Early ear development in the embryo of the zebrafish, Danio rerio." J Comp Neurol **365**(1): 113-128.

Hammond, K. L., H. E. Loynes, A. A. Folarin, J. Smith and T. T. Whitfield (2003). "Hedgehog signalling is required for correct anteroposterior patterning of the zebrafish otic vesicle." Development **130**(7): 1403-1417.

Hans, S., D. Liu and M. Westerfield (2004). "Pax8 and Pax2a function synergistically in otic specification, downstream of the Foxi1 and Dlx3b transcription factors." Development **131**(20): 5091-5102.

Hashimoto, M., K. Shinohara, J. Wang, S. Ikeuchi, S. Yoshiba, C. Meno, S. Nonaka, S. Takada, K. Hatta, A. Wynshaw-Boris and H. Hamada (2010). "Planar polarization of node cells determines the rotational axis of node cilia." Nat Cell Biol **12**(2): 170-176.

Heath, K. E., A. Campos-Barros, A. Toren, G. Rozenfeld-Granot, L. E. Carlsson, J. Savige, J. C. Denison, M. C. Gregory, J. G. White, D. F. Barker, A. Greinacher, C. J. Epstein, M. J. Glucksman and J. A. Martignetti (2001). "Nonmuscle myosin heavy chain IIA mutations define a spectrum of autosomal dominant macrothrombocytopenias: May-Hegglin anomaly and Fechtner, Sebastian, Epstein, and Alport-like syndromes." Am J Hum Genet **69**(5): 1033-1045.

Hirota, Y., A. Meunier, S. Huang, T. Shimozawa, O. Yamada, Y. S. Kida, M. Inoue, T. Ito, H. Kato, M. Sakaguchi, T. Sunabori, M. A. Nakaya, S. Nonaka, T. Ogura, H. Higuchi, H. Okano, N. Spassky and K. Sawamoto (2010). "Planar polarity of multiciliated ependymal cells involves the anterior migration of basal bodies regulated by non-muscle myosin II." Development 137(18): 3037-3046.

Huang, Y., X. Wang, X. Wang, M. Xu, M. Liu and D. Liu (2013). "Nonmuscle myosin II-B (myh10) expression analysis during zebrafish embryonic development." Gene Expr Patterns **13**(7): 265-270.

Inoue, M., M. Tanimoto and Y. Oda (2013). "The role of ear stone size in hair cell acoustic sensory transduction." Sci Rep **3**: 2114.

Ishikawa, H. and W. F. Marshall (2011). "Ciliogenesis: building the cell's antenna." Nat Rev Mol Cell Biol **12**(4): 222-234.

Iwai, S., D. Hanamoto and S. Chaen (2006). "A point mutation in the SH1 helix alters elasticity and thermal stability of myosin II." J Biol Chem **281**(41): 30736-30744.

Jacobson, A. G. (1963). “The determination and positioning of the nose, lens, and the ear.” J Exp Zool **154**: 273-283.

Karavitaki, K. D. and D. P. Corey (2010). "Sliding adhesion confers coherent motion to hair cell stereocilia and parallel gating to transduction channels." J Neurosci **30**(27): 9051-9063.

Kernan, M. and C. Zuker (1995). "Genetic approaches to mechanosensory transduction." Curr Opin Neurobiol **5**(4): 443-448.

Kimmel, C. B., W. W. Ballard, S. R. Kimmel, B. Ullmann and T. F. Schilling (1995). "Stages of embryonic development of the zebrafish." Dev Dyn **203**(3): 253-310.

Kimmel, C. B., J. Patterson and R. O. Kimmel (1974). "The development and behavioral characteristics of the startle response in the zebra fish." Dev Psychobiol **7**(1): 47-60.

Kovacs, M., J. Toth, C. Hetenyi, A. Malnasi-Csizmadia and J. R. Sellers (2004). "Mechanism of blebbistatin inhibition of myosin II." J Biol Chem **279**(34): 35557-35563.

Kunishima, S. and H. Saito (2010). "Advances in the understanding of MYH9 disorders." Curr Opin Hematol **17**(5): 405-410.

Lalwani, A. K., J. A. Goldstein, M. J. Kelley, W. Luxford, C. M. Castelein and A. N. Mhatre (2000). "Human nonsyndromic hereditary deafness DFNA17 is due to a mutation in nonmuscle myosin MYH9." Am J Hum Genet **67**(5): 1121-1128.

Lalwani, A. K., F. H. Linthicum, E. R. Wilcox, J. K. Moore, F. C. Walters, T. B. San Agustin, J. Mislinski, M. R. Miller, Y. Sinninger, A. Attaie and W. M. Luxford (1997). "A five-generation family with late-onset progressive hereditary hearing impairment due to cochleosaccular degeneration." Audiol Neurootol **2**(3): 139-154.

Lalwani, A. K., W. M. Luxford, A. N. Mhatre, A. Attaie, E. R. Wilcox and C. M. Castelein (1999). "A new locus for nonsyndromic hereditary hearing impairment, DFNA17, maps to chromosome 22 and represents a gene for cochleosaccular degeneration." Am J Hum Genet **64**(1): 318-323.

Lemullois, M., C. Klotz and D. Sandoz (1987). "Immunocytochemical localization of myosin during ciliogenesis of quail oviduct." Eur J Cell Biol **43**(3): 429-437.

Liu, D., H. Chu, L. Maves, Y. L. Yan, P. A. Morcos, J. H. Postlethwait and M. Westerfield (2003). "Fgf3 and Fgf8 dependent and independent transcription factors are required for otic placode specification." Development **130**(10): 2213-2224.

Lo, C. M., D. B. Buxton, G. C. Chua, M. Dembo, R. S. Adelstein and Y. L. Wang (2004). "Nonmuscle myosin IIb is involved in the guidance of fibroblast migration." Mol Biol Cell **15**(3): 982-989.

Lopez-Schier, H., C. J. Starr, J. A. Kappler, R. Kollmar and A. J. Hudspeth (2004). "Directional cell migration establishes the axes of planar polarity in the posterior lateral-line organ of the zebrafish." Dev Cell **7**(3): 401-412.

Marshall, W. F. and C. Kintner (2008). "Cilia orientation and the fluid mechanics of development." Curr Opin Cell Biol **20**(1): 48-52.

Mhatre, A. N., J. Li, Y. Kim, D. E. Coling and A. K. Lalwani (2004). "Cloning and developmental expression of nonmuscle myosin IIA (Myh9) in the mammalian inner ear." J Neurosci Res **76**(3): 296-305.

Mhatre, A. N., Y. Li, G. Atkin, A. Maghnouj and A. K. Lalwani (2006). "Expression of Myh9 in the mammalian cochlea: localization within the stereocilia." J Neurosci Res **84**(4): 809-818.

Mhatre, A. N., Y. Li, N. Bhatia, K. H. Wang, G. Atkin and A. K. Lalwani (2007). "Generation and characterization of mice with Myh9 deficiency." Neuromolecular Med **9**(3): 205-215.

Mirkovic, I., S. Pylawka and A. J. Hudspeth (2012). "Rearrangements between differentiating hair cells coordinate planar polarity and the establishment of mirror symmetry in lateral-line neuromasts." Biol Open **1**(5): 498-505.

Mirzadeh, Z., Y. G. Han, M. Soriano-Navarro, J. M. Garcia-Verdugo and A. Alvarez-Buylla (2010). "Cilia organize ependymal planar polarity." J Neurosci **30**(7): 2600-2610.

Morton, C. C. and W. E. Nance (2006). "Newborn hearing screening--a silent revolution." N Engl J Med **354**(20): 2151-2164.

Murayama, S., M. Akiyama, H. Namba, Y. Wada, H. Ida and S. Kunishima (2013). "Familial cases with MYH9 disorders caused by MYH9 S96L mutation." Pediatr Int **55**(1): 102-104.

Nance, W. E. (2003). "The genetics of deafness." Ment Retard Dev Disabil Res Rev **9**(2): 109-119.

Nicolson, T. (2005). "The genetics of hearing and balance in zebrafish." Annu Rev Genet **39**: 9-22.

Noden, D. M. (1986). "Origins and patterning of craniofacial mesenchymal tissues." J Craniofac Genet Dev Biol Suppl **2**: 15-31.

Nonaka, S., S. Yoshiba, D. Watanabe, S. Ikeuchi, T. Goto, W. Marshall and H. Hamada (2005). "De novo formation of left-right asymmetry by posterior tilt of nodal cilia." PLoS Biol **3**(8): e268.

Odronitz, F. and M. Kollmar (2007). "Drawing the tree of eukaryotic life based on the analysis of 2,269 manually annotated myosins from 328 species." Genome Biol **8**(9): R196.

Okada, Y., S. Takeda, Y. Tanaka, J. C. Izpisua Belmonte and N. Hirokawa (2005). "Mechanism of nodal flow: a conserved symmetry breaking event in left-right axis determination." Cell **121**(4): 633-644.

Pisam, M., C. Jammet and D. Laurent (2002). "First steps of otolith formation of the zebrafish: role of glycogen?" Cell Tissue Res **310**(2): 163-168.

Platt, C. (1993). "Zebrafish inner ear sensory surfaces are similar to those in goldfish." Hear Res **65**(1-2): 133-140.

Quarmby, L. M. and J. D. Parker (2005). "Cilia and the cell cycle?" J Cell Biol **169**(5): 707-710.

Ricketson, D., C. A. Johnston and K. E. Prehoda (2010). "Multiple tail domain interactions stabilize nonmuscle myosin II bipolar filaments." Proc Natl Acad Sci U S A **107**(49): 20964-20969.

Riley, B. B. and B. T. Phillips (2003). "Ringing in the new ear: resolution of cell interactions in otic development." Dev Biol **261**(2): 289-312.

Riley, B. B., C. Zhu, C. Janetopoulos and K. J. Aufderheide (1997). "A critical period of ear development controlled by distinct populations of ciliated cells in the zebrafish." Dev Biol **191**(2): 191-201.

Robu, M. E., J. D. Larson, A. Nasevicius, S. Beiraghi, C. Brenner, S. A. Farber and S. C. Ekker (2007). "p53 activation by knockdown technologies." PLoS Genet **3**(5): e78.

Saitoh, T., S. Takemura, K. Ueda, H. Hosoya, M. Nagayama, H. Haga, K. Kawabata, A. Yamagishi and M. Takahashi (2001). "Differential localization of non-muscle myosin II isoforms and phosphorylated regulatory light chains in human MRC-5 fibroblasts." FEBS Lett **509**(3): 365-369.

Sanborn, K. B., E. M. Mace, G. D. Rak, A. Difeo, J. A. Martignetti, A. Pecci, J. B. Bussel, R. Favier and J. S. Orange (2011). "Phosphorylation of the myosin IIA tailpiece regulates single myosin IIA molecule association with lytic granules to promote NK-cell cytotoxicity." Blood **118**(22): 5862-5871.

Satir, P. and S. T. Christensen (2007). "Overview of structure and function of mammalian cilia." Annu Rev Physiol **69**: 377-400.

Sawamoto, K., H. Wichterle, O. Gonzalez-Perez, J. A. Cholfin, M. Yamada, N. Spassky, N. S. Murcia, J. M. Garcia-Verdugo, O. Marin, J. L. Rubenstein, M. Tessier-Lavigne, H. Okano and A. Alvarez-Buylla (2006). "New neurons follow the flow of cerebrospinal fluid in the adult brain." Science **311**(5761): 629-632.

Schartl, M. (2014). "Beyond the zebrafish: diverse fish species for modeling human disease." Dis Model Mech **7**(2): 181-192.

Scholey, J. M., I. Brust-Mascher and A. Mogilner (2003). "Cell division." Nature **422**(6933): 746-752.

Seiler, C., O. Ben-David, S. Sidi, O. Hendrich, A. Rusch, B. Burnside, K. B. Avraham and T. Nicolson (2004). "Myosin VI is required for structural integrity of the apical surface of sensory hair cells in zebrafish." Dev Biol **272**(2): 328-338.

Seri, M., R. Cusano, S. Gangarossa, G. Caridi, D. Bordo, C. Lo Nigro, G. M. Ghiggeri, R. Ravazzolo, M. Savino, M. Del Vecchio, M. d'Apolito, A. Iolascon, L. L. Zelante, A. Savoia, C. L. Balduini, P. Noris, U. Magrini, S. Belletti, K. E. Heath, M. Babcock, M. J. Glucksman, E. Aliprandis, N. Bizzaro, R. J. Desnick and J. A. Martignetti (2000). "Mutations in MYH9 result in the May-Hegglin anomaly, and Fechtner and Sebastian syndromes. The May-Heggllin/Fechtner Syndrome Consortium." Nat Genet **26**(1): 103-105.

Smith, D. J., A. A. Smith and J. R. Black (2011). "Mathematical embryology: the fluid mechanics of nodal cilia." Tuck Memorial Issue of the Journal of Engineering Mathematics.

Solecki, D. J., N. Trivedi, E. E. Govek, R. A. Kerekes, S. S. Gleason and M. E. Hatten (2009). "Myosin II motors and F-actin dynamics drive the coordinated movement of the centrosome and soma during CNS glial-guided neuronal migration." Neuron **63**(1): 63-80.

Sollner, C., M. Burghammer, E. Busch-Nentwich, J. Berger, H. Schwarz, C. Riekel and T. Nicolson (2003). "Control of crystal size and lattice formation by starmaker in otolith biomineralization." Science **302**(5643): 282-286.

Sollner, C., G. J. Rauch, J. Siemens, R. Geisler, S. C. Schuster, U. Muller and T. Nicolson (2004). "Mutations in cadherin 23 affect tip links in zebrafish sensory hair cells." Nature **428**(6986): 955-959.

Sprague, J., L. Bayraktaroglu, D. Clements, T. Conlin, D. Fashena, K. Frazer, M. Haendel, D. G. Howe, P. Mani, S. Ramachandran, K. Schaper, E. Segerdell, P. Song, B. Sprunger, S. Taylor, C. E. Van Slyke and M. Westerfield (2006). "The Zebrafish Information Network: the zebrafish model organism database." Nucleic Acids Res **34**(Database issue): D581-585.

Stooke-Vaughan, G. A., P. Huang, K. L. Hammond, A. F. Schier and T. T. Whitfield (2012). "The role of hair cells, cilia and ciliary motility in otolith formation in the zebrafish otic vesicle." Development **139**(10): 1777-1787.

Svitkina, T. M., A. B. Verkhovsky, K. M. McQuade and G. G. Borisy (1997). "Analysis of the actin-myosin II system in fish epidermal keratocytes: mechanism of cell body translocation." J Cell Biol **139**(2): 397-415.

Svoboda, K. and S. M. Block (1994). "Biological applications of optical forces." Annu Rev Biophys Biomol Struct **23**: 247-285.

Tanimoto, M., Y. Ota, M. Inoue and Y. Oda (2011). "Origin of inner ear hair cells: morphological and functional differentiation from ciliary cells into hair cells in zebrafish inner ear." J Neurosci **31**(10): 3784-3794.

Thomas, A. J., D. W. Hailey, T. M. Stawicki, P. Wu, A. B. Coffin, E. W. Rubel, D. W. Raible, J. A. Simon and H. C. Ou (2013). "Functional mechanotransduction is required for cisplatin-induced hair cell death in the zebrafish lateral line." J Neurosci **33**(10): 4405-4414.

Tian, T., L. Zhao, X. Zhao, M. Zhang and A. Meng (2009). "A zebrafish gene trap line expresses GFP recapturing expression pattern of foxj1b." J Genet Genomics **36**(10): 581-589.

Torres, M. and F. Giraldez (1998). "The development of the vertebrate inner ear." Mech Dev **71**(1-2): 5-21.

Vicente-Manzanares, M., X. Ma, R. S. Adelstein and A. R. Horwitz (2009). "Non-muscle myosin II takes centre stage in cell adhesion and migration." Nat Rev Mol Cell Biol **10**(11): 778-790.

Walsh, E. C. and D. Y. Stainier (2001). "UDP-glucose dehydrogenase required for cardiac valve formation in zebrafish." Science **293**(5535): 1670-1673.

Whitfield, T. T., B. B. Riley, M. Y. Chiang and B. Phillips (2002). "Development of the zebrafish inner ear." Dev Dyn **223**(4): 427-458.

Wu, D., J. B. Freund, S. E. Fraser and J. Vermot (2011). "Mechanistic basis of otolith formation during teleost inner ear development." Dev Cell **20**(2): 271-278.

Xiao, M., J. G. Reifenberger, A. L. Wells, C. Baldacchino, L. Q. Chen, P. Ge, H. L. Sweeney and P. R. Selvin (2003). "An actin-dependent conformational change in myosin." Nat Struct Biol **10**(5): 402-408.

Yu, X., D. Lau, C. P. Ng and S. Roy (2011). "Cilia-driven fluid flow as an epigenetic cue for otolith biomineralization on sensory hair cells of the inner ear." Development **138**(3): 487-494.

Yu, X., C. P. Ng, H. Habacher and S. Roy (2008). "Foxj1 transcription factors are master regulators of the motile ciliogenic program." Nat Genet **40**(12): 1445-1453.

Yumura, S. and T. Q. Uyeda (2003). "Myosins and cell dynamics in cellular slime molds." Int Rev Cytol **224**: 173-225.

Zinchuk, V. and O. Zinchuk (2008). "Quantitative colocalization analysis of confocal fluorescence microscopy images." Curr Protoc Cell Biol **Chapter 4**: Unit 4 19.